KERNFORSCHUNGSANLAGE JÜLICH GmbH
Projekt Spallations-Neutronenquelle
Zentralabteilung Allgemeine Technologie

Experimental Determination of the Local Heat Transfer Coefficient in a Closely Packed Pin Arrangement

by

S. V. Möller

Jül - Spez - 173
September 1982
ISSN 0343-7639

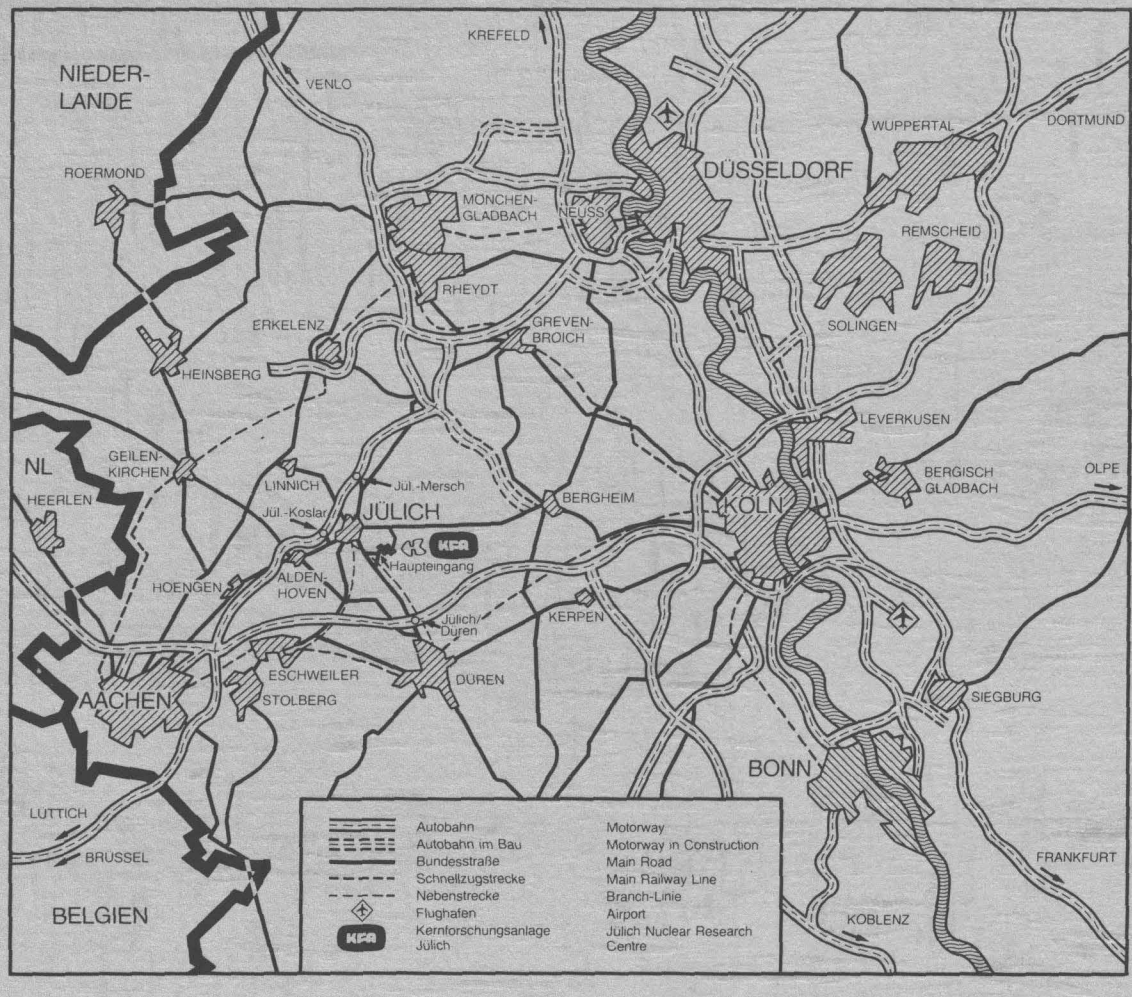

Als Manuskript gedruckt

Spezielle Berichte der Kernforschungsanlage Jülich — Nr. 173

Projekt Spallations-Neutronenquelle

Zentralabteilung Allgemeine Technologie

Jül - Spez - 173

Zu beziehen durch: ZENTRALBIBLIOTHEK der Kernforschungsanlage Jülich GmbH

Postfach 1913 · D-5170 Jülich (Bundesrepublik Deutschland)

Telefon: 02461/610 · Telex: 833556 kfa d

Experimental Determination of the Local Heat Transfer Coefficient in a Closely Packed Pin Arrangement

by

S. V. Möller

M. SC. Sergio Viçosa Möller

Instituto de Engenharia Nuclear Comissão Nacional de Energia Nuclear
Rio de Janeiro – Brazil

Abstract

The determination of the heat transfer coefficient of the pins of the Spallation Neutron Source is a very important problem for the development of this facility, as data for thermal and structural studies.

For this purpose, a test apparatus was built, in scale 1 : 1, for the simulation of the thermal and hydraulical conditions of the Neutron Source. This apparatus is a pin bank, with one of the pins electrically heated.

Performance of measurements gave the values for the heat transfer coefficient, here presented in the Nusselt Number form, and its local distribution.

Results show the linear dependence of Nusselt Number on Reynolds Number, for a constant heat production.

Zusammenfassung

Die Bestimmung des Wärmeübergangskoeffizienten an den Targetstäben ist eine wesentliche Vorraussetzung für die Auslegung einer Spallations-Neutronenquelle und bildet die Grundlage für thermische und mechanische Berechnungen.
Zu diesem Zwecke wurde eine Meßapparatur im Maßstab 1 : 1 gebaut, an der die thermischen und hydraulischen Verhältnisse der Spallations-Neutronenquelle teilweise simuliert werden. Hierbei handelt es sich um eine Anordnung mehrerer Targetstäbe, von denen ein Stab elektrisch beheizt wird.
Die Messungen lieferten Wärmeübergangskoeffizienten, die in Form der Nusselt Zahl dargestellt werden, wobei auch die örtliche Verteilung berücksichtigt wurde, sich bei konstanten Heizleistungen eine lineare Abhängigkeit für Nusselt von Reynolds.

Acknowledgements

Author wishes to thanks the International Atomic Energy Agency - IAEA, the Kernforschungsanlage-Jülich - KFA-Jülich, and the Comissao Nacional de Energia Nuclear - CNEN in Brazil, who sponsored this training at the Zentralabteilung Allgemeine Technologie - ZAT/KFA-Jülich, where this work was done.

Thanks to Dipl.-Ing. Horst Stechemesser, Author's Adviser, whose orientation made this work become possible.

Thanks also to Dr. Stelzer and Mr. Sievers for their help with the computer work, and to Mr. Beuth and Mr. Greiß for the help with the measurements.

Special thanks to Mr. Hellenbrandt, who assembled with skill the test apparatus and helped Author performing the long runs of the experiment.

To Miss Bellartz thanks for the typewriting of the manuscripts.

Index

1. Introduction

Objective of this report is to present the results of measurements performed in the dependences of the Central Department for General Technology (ZAT) of the Nuclear Research Center Jülich (KFA), in order to determine the heat transfer conditions of the pin bank target of the German Spallation Neutron Source.

This facility is a rotating wheel shaped target /1/, where a bank of water cooled lead pins, each one protected by an aluminium cladding, is hit by a proton beam of medium energy to produce a neutron flux equivalent to $7.10^{14} cm^{-2} s^{-1}$ and a maximum of $1,3.10^{16} cm^{-2} s^{-1}$ /2/. Figure 1 describes the spallation process for a heavy nucleus, as lead, and the alternative mode, using Uran-238. Figure 2 shows the rotating target wheel.

For the purpose of this work it was built in KFA-Jülich a test apparatus simulating a group of pins of the target wheel. These pins are placed in a rectangular channel in crossflow of water, being one of these pins electrically heated. The study of the thermal behaviour of this pin will lead to the determination of the characteristics of the heat transfer process in the target wheel, that means, the heat transfer coefficient.

The results obtained along this experiment will be used as datas for a calculation through the Finite-Element-Method /3/, the comparision of both temperature fields will be taken as guide for the exactness of the measurements.

The heat transfer coefficient obtained from this experiments can be used further to complement studies of temperature and stresses distribution in the pins of the Spallation /4/.

2. Description of the Experimemt

2.1 The Test Apparatus

Figures 3 and 4 show the Test Apparatus, which consists on a rectangular channel where a bank of 32 pins in staggered arrangement is placed in crossflow of water. One of this pins, in the fifth row, is made of graphit and electrically heated, the others are made of aluminium, except those surrounding the graphit pin which should formerly also be heated, but this point will be discussed furtherly.

The heated pin, shown on figure 5, is instrumented by two pairs of thermocouples, opposed 180^{o}. In each pair, one thermocouple lies on the internal surface, and the other is introduced inside graphit almost until external surface, as shown on figure 6. This pin can be rotated around its own axis to permit measurement on several angles with respect to the point of incidence of the flow.

Measurement of cooling water temperature is made by two Thermocouples placed at water inlet and outlet.

The rate of cooling water is measured with help of a Float-Type Flowmeter (Rotameter).

The test apparatus is placed in a tank with demineralized water in order to cool plexiglass upper and lower walls, which provide insulation between the graphit pin and the apparatus. The reason of using demineralized water, not only in the tank, but also for cooling the pins, is to avoid electrolisis in the whole system.

Dimensions and equipments for the test apparatus are listed on Table 1, remarking that the pins in the test apparatus have the same dimensions as in the Target Wheel.

2.2 Test Procedure

For a certain known angle of thermocouples in the heated pin, as shown on figure 6, a value for the electrical current through the pin is set and the flowrate variated over a certain range, then, a new value for the current is adjusted and the flowrate variated again, and so on. This procedure is followed for several angles of thermocouples from 0^{o} to 180^{o}, being water temperature measured at each step.

The heat production is calculated by means of the electrical current and the electricial resistivity of graphit.

The heat transfer coefficient is determined by means of the temperature on the external surface of the pin, heat generation intensity, water temperature and flowrate.

Measurement of the temperature of the internal surface of the pin, which is insulated by sylicon rubber, and inside the pin will lead to the value of the temperatue on its external surface, which is directly in contact with water.

The decision of running the experiment with only one heated pin was taken because the ideal situation was measuring the temperature on pin's surface and cooling water at the same angle, as shown schematically on figure 7, but this is not possible, without disturbing the flow, due to the small distance between pins. The alternative is the determination of the heat transfer using the mean value of inlet and outlet water temperature. If the seven pins were heated, the temperature gradient along the flow in the vicinity of the pin would be stronger

than if only one pin were heated. In this case, the stream, showed by dotted line on Figure 7, would help to keep the temperature gradient lighter than with 7 pins.

The second advantage of running the experiment with only one heated pin was the lower thermal load on the plexiglass plates, and smaller possibility of electrolysis, which proportioned a longer durability of the apparatus.

Nevertheless, theseassumptions were checked, by comparision of the readings,before adopted.

2.3 Sources of Errors

The main difficulty of this experiment is the correct measurement of the temperature inside graphit wall. Many factors /5/ contribute to increase this difficulty. The first is the uncertainty of the position of the measuring junction inside the thermocouple itself and its position inside the pin. The second factor is that the thermal gradient along the thermocouple may not be equal to the gradient across the wall due to the different thermal conductivity of both materials and the absence of heat generation in the thermocouple.

The measurement of the temperature of the internal surface can be influenced by the existence of thermal gradients on this surface in angular direction, because of the difficulty on positioning the thermocouple along an isotherm, which coincides with a generatrix of the cylindrical surface. Nevertheless, this influence is not so strong as in the measurement of the temperature inside the wall because this temperature gradient is lighter.

Measurement of cooling water temperature offers no difficulty. Effect of gradients along the thermocouple can be minimized by

imersing the thermocouple deep inside the stream, and besides, the difference between cooling and tank water temperature is not great.

Accuracy of flowrate measurement is affected in two ways, the first is the accuracy range of the flowmeter, the second is the reading of the flowrate which is affected by the oscilation of the floater due to fluctuations of the flowrate.

3. Mathematical Analysis

General Equation for Heat Conduction in cylindrical coordinates /6/ is

$$\frac{\partial T}{\partial t} = \alpha \left(\frac{\partial^2 T}{\partial r^2} + \frac{I}{r}\frac{\partial T}{\partial r} + \frac{I}{r^2}\frac{\partial^2 T}{\partial \theta^2} + \frac{\partial^2 T}{\partial Z^2}\right) + \frac{\dot{q}}{\rho Cp} \tag{1}$$

or

$$\frac{I}{\alpha}\frac{\partial T}{\partial t} = \frac{\partial^2 T}{\partial r^2} + \frac{I}{r}\frac{\partial T}{\partial r} + \frac{I}{r^2}\frac{\partial^2 T}{\partial \theta^2} + \frac{\partial^2 T}{\partial Z^2} + \frac{\dot{q}}{\lambda} \tag{2}$$

where $\dot{q}$ is the intensity of the heat source.

Considering this analysis for the regions of the pin not close to its extremities, one can assume that no heat flows in the axial direction, so

$$\frac{\partial^2 T}{\partial Z^2} = O \tag{3}$$

Assuming also that the system is on steady state

$$\frac{\partial T}{\partial t} = O \tag{4}$$

from Eqs. (3) and (4), Equation (2) becomes

$$\frac{\partial^2 T}{\partial r^2} + \frac{I}{r}\frac{\partial T}{\partial r} + \frac{I}{r^2}\frac{\partial^2 T}{\partial \theta^2} = -\frac{\dot{q}}{\lambda} \tag{5}$$

As stated in 2., the internal surface of the pin is insulated, and heat flows through the external surface by forced convection to the water. It is intuitive that the heat transfer coefficient α is function of the position, in this problem θ, shown in Figure 8.

The simmetry leads to the assumption that no heat flows in the angular direction for θ equal to 0^{o} and 180^{o}.

So, boundary conditions for the problem are:

$$r = r_i \ , \quad \text{any } \theta \ , \quad \frac{\partial T}{\partial r} = 0 \tag{6-a}$$

$$r = r_e, \quad \text{any } \theta \ , \quad \lambda \frac{\partial T(\theta)}{\partial r} = \alpha_\theta \ (Tw(\theta) - T_\infty) \tag{6-b}$$

$$\text{any } r, \quad \theta = 0^{o}, \ \frac{\partial T}{\partial \theta} = 0 \tag{6-c}$$

$$\text{any } r, \quad \theta = 180^{o}, \ \frac{\partial T}{\partial \theta} = 0 \tag{6-d}$$

where

λ. thermal conductivity of graphit

Tw. temperature of the surface in contact with water

T_∞. undisturbed temperature of the fluid (infinite)

α_θ. local heat transfer coefficient

Literature gives many empirical equations for the heat transfer coefficient. Being

$$\bar{\alpha} = \frac{1}{\theta} \int_{0^{o}}^{180^{o}} \alpha_\theta \ d\theta \tag{7}$$

its value /7/ can be given by

$$\bar{\alpha} = \frac{\lambda f}{d} \; 0{,}35 \left(\frac{p}{d}\right)^{0,2} R_{e\infty}^{0,6} \; Pr_{\infty}^{0,36} \left(\frac{Pr_{\infty}}{Prw}\right)^{0,25} \qquad (8)$$

where

λf - thermal conductivity of the fluid
Re_{∞} - Reinolds's Number at infinite
Pr_{∞} - Prandtl's Number at infinite
Prw - Prandtl's Number calculated at wall temperature
Being the Nusselt's Number for this problem

$$Nu = \frac{\bar{\alpha} d}{\lambda f} \qquad (9)$$

and considering the influence of the heat production, Equation (8) can be plotted as shown on Figure 9.

Figure 10 shows the variation of heat transfer coefficient as function of θ for a tube in a staggered bank, according to Zukauskas /7/.

The same analysis can be done for the Spallation's pins, where the target material is lead or U. 238, protected by an aluminium cladding.

As mentioned before, measurement of the temperature on the internal surface and inside pin's wall allows the determination of the temperature on the external surface. This can be made through the equation for the temperature profile in a hollowed cylinder with uniform heat source distribution and two fixed temperatures in two different well known points /6/

$$Tw = Ti + (T_t - T_i) \frac{\ln (r_e/r_i)}{\ln (r_t/r_i)} +$$

$$\frac{\dot{q}}{4\lambda} (r_t^2 - r_i^2) \frac{\ln (r_e/r_i)}{\ln (r_t/r_i)} - (r_e^2 - r_i^2) \qquad (10)$$

Where

T_i - temperature on internal surface (measured)

T_t - temperature inside pin's wall (measured)

r_t - radius of the position of the measuring junction of the thermocouple inside pin's wall.

This equation does not take in account the heat flux in the angular direction, nevertheless, it is valid along a radius for a certain known angle, even with heat flux in the angular direction, for two fixed known temperatures.

4. Results of the experiment

4.1 Method of analysis

Table 2 lists the conditions for each step of the execution of this experiment.

Calculation of the Heat Power was done through

$$W = Ri^2 \tag{11}$$

or

$$\dot{q} = Ri^2/V \tag{12}$$

where

W - heat production - W
i - electrical current - A
v - volume of the graphit pin - mm^3
R - electrical resistivity of the whole pin, shown on Figure 11, and given by

$$R = 12.36\text{-}0{,}013\ \bar{T} \quad (m\ \Omega) \tag{13}$$

where

$\bar{T}$ - mean temperature of the pin

For the calculation of the temperature on the external surface through Equation (10), the thermal conductivity of graphit, shown on Figure 12, is given by

$$\lambda = 24{,}4\ e^{-1{,}08704.10^{-3}\ T}\ (W/m^{o}k) \tag{14}$$

Figures 13 and 14 show the X-Ray pictures of the pins and their thermocouples. As one can see, the position of the measuring junction is not defined, but only the region where the junction is placed can be determined. Therefore, by calculating the temperature on the external surface of the pin, through Equation (10), two different values for r_t must be taken for each case, as shown on both Figures 13 and 14 for each pair of thermocouples, which will lead to two different temperatures for the same case.

The consequence of this procedure will be, in each case, a band limited by a maximum and a minimum value. In those well defined region lie the actual values for each physical quantity analyzed.

The determination of the heat transfer coefficient was made by means of the meat flux through the wall

$$\underset{\sim}{q} = \frac{\dot{q}A}{P} \quad (W/mm^2) \tag{15}$$

Where

$\underset{\sim}{q}$ - is the heat flux
A - area of the cross section of the pin
P - external perimeter of the pin and the heat transfer

coefficient is calculated by

$$\bar{\alpha} = \frac{\underset{\sim}{q}}{Tw-T_\infty} \quad W/mm^2\ k \tag{16}$$

Where Tw is the average of the temperatures obtained for each angle using its maximum and minimum value, and T_∞ is the average of water inlet and outlet temperatures.

Values for physical properties of water were taken from Reference 3.

4.2 Analysis of the Results

Tables 3 to 11 list the results obtained through this experiment.

In the first column of each table are the values for the Reynolds Number obtained form each one of the flowrates shown on Table 2

The second column shows the values of the heat production. These values are not constant along the column because of the different mean temperature $\bar{T}$ (see Equation 11) of the pin, due to different cooling ratios for each Re.

The 3^{rd} to 9^{th} columns show the overtemperatures (difference between the local temperature of the surface of the pin and the water temperature) for several angles between 0^{o} and 180^{o}.

The last column shows the Nusselt Number, calculated by means of Equation (9), for each line, taking $\bar{\alpha}$ as given by Equation (16).

Figures 15 to 19 show the temperature distribution on the external surface according to the datas given on Table 11, where the heat production W is about 7,3 kW. In these curves one can see clearly the effect of not determining correctly the position of the measuring junction of the thermocouples inside pin's wall. The smaller value for r_t, shown for each angle on Figures 13 and 14, leads to the line of lower temperature and its greater value to the line of higher temperature. Another point that can be seen in these graphics is that the temperature profiles are becoming smoother as the Reynolds Number increases.

Figures 20 to 24 show the behaviour of the Nusselt Number as function of the heat production taking the Reynolds Number as parameter. Due the fact that the Reynolds Number varies because the temperature of the water oscilates, an average value was taken. One can see also that the oscillatory behavior of the Nusselt Number for low values of the heat production is dumped as the latter increases.

Figures 25 to 33 show the behaviour of the Nusselt Number as function of the Reynolds Number, taking the heat production as parameter. These graphics show clearly the linear dependence of the Nusselt Number on the Reynolds Number.

Figures 34 to 38 show the variation of the heat transfer coefficient as a function of the position, remaking that $\theta = 0^{o}$ coincides with the point of incidence of the flow. Since these curves were obtained from the temperatures shown on Figures 15 to 19, they have the same tendence on become smoother as the Reynolds Number increases.

In this experiment the influence of the Prandtl Number was not observed. The Prandtl Number, in such an experiment, is used to express the influence of the difference between fluid and wall temperature as seen in Equation (8). The reason is that in this case, this temperature difference is consequence of the heat production, and besides, the results are more useful if expressed in therms of the heat production than in therms of Prandtl Number.

4.3 Comparision with the literature

Through an iterative method, Equation (8) was used to determine the heat transfer coefficient for the same conditions that the experiment was performed, this iteration is needed because the

temperature of the external surface, for the calculation of Pr_w, is not known. Figure 39 shows the heat transfer coefficient as function of the flowrate and the curve obtained through Equation (8). As one can see they do not agree, but this can be explained by the fact that Equation (8) is obtained from empirical results for pitch to diameter ratios greater than the actual relation (1,04).

Curves shown on Figures 34 to 38 for the local heat transfer coefficient do not agree with the curve for a tube in a staggered bank proposed by Zukauskas /7/ and the reason is still the small value of the pitch to diameter ratio of the pins of this experiment in comparision to those in Reference /7/.

4.4 Counter calculation

In order to check the results one of the temperature distributions on the external surface and the respective heat transfer coefficient was taken to be analyzed through the Finite-Element-Method by means of program FEMFAM-T /8/. The case chosed was that with the maximum heat production achieved (73272 W) and the highest Reynolds Number (73246).

For the simplification of the calculation the heat transfer distribution shown on Figure 38 will be substituted by the stepwise approximation shown on Figure 40.

Figure 41 shows the mesh used for the calculation and presents the temperature for each knot. The value of the heat transfer coefficient used is

$$\bar{\alpha} = 1,272 \text{ W/cm}^{2o}\text{k}$$

or

$$Nu = 506,2$$

and the point of incidence of the flow is the knot number 49.

Due to the simmetry, only one side of the pin was taken.

Figures 42 and 43 illustrate the results of this calculation and show the temperature field of the pin.

Figure 44 shows the isotherms for this case.

The second value for the heat transfer coefficient for this case is

$$\bar{\alpha} = 1,145 \text{ W/cm}^{2o}\text{k}$$

or

$$Nu = 455,7$$

The temperature field obtained with this $\bar{\alpha}$ is shown, with the mesh, in Figure 45, and is illustrated by Figures 46 and 47, being the isotherms shown on Figure 48.

Results of both calculations can be compared to the temperature profile presented on Table 11, or directly to the curves; by Figure 49. In this figure the curves obtained through FEMFAM-T are superimposed to those obtained experimentally, being the latters showed with the experimental points (stars).

The fact that the curves obtained numerically being smoother than the experimental ones is due to the stepwise approximation, shown on Figure 38, for the heat transfer coefficient distribution.

5. Conclusions

It was not possible, because of the constructive characteristics of the test apparatus, to achieve the same heat generation level expected for the pins of the Spallation Neutron Source, but the results obtained through this experiment and presented on Chapter 4 can be extrapolated to 8,5 kw, because they cover a wide range of heat generation intensity from 0,12 to 7,37 kw.

The results are presented in form of bands limited by lines obtained with the experimental points. This is due to the method used for the measurement of the temperature inside graphit wall. Without changing the method, this could be minimized using thermocouples with smaller diameters, from this procedure a narrower band would result. Nevertheless these bands are very well defined and can be used in further thermal and structural studies for the Spallation Neutron Source.

Nomenclature

A - area of the cross section of the pin
Cp - specific heat
d - external diameter of the pin
i - electrical current,
p - pitch
P - perimeter of the pin
θ - flowrate, m^3/h
$\dot{q}$ - intensity of the heat source, W/mm^3
$\underset{\sim}{q}$ - heat flux through the wall, W/mm^2
r - radius (cylindrical coordinates)
r_i - internal radius of the pin
r_e - external radius of the pin
r_t - radius of the position of the measuring junction of the thermocouple
R - electrical resistivity of graphit
t - time (in equation of the heat conduction)
T - temperature
Tw - temperature of the surface of the pin in contact with water
T_∞ - undisturbed water temperature
$\bar{T}$ - mean temperature of the graphit pin
V - volume of the graphit pin
w - heat production, watts
Z - coordinate (cylindrical coordinates)
Re_∞ - Reynolds Number at infinite
Pr_w - Prandtl Number at wall temperature
Pr_∞ - Prandtl Number at infinite
N_u - Nusselt Number
α_θ - Local heat transfer coefficient, W/cm^2k
$\bar{\alpha}$ - General heat transfer coefficient, W/cm^2k
α - $\rho c\phi/\lambda$ - thermal permissivity
θ - coordinate (cylindrical coordinates)
θ - angle of the position with respect to the point of incidence of the flow at pin
ρ - density of water
λ - thermal conductivity of graphit
λf - thermal conductivity of water

References

1. Bauer, G. and Stechemesser, H. - "Mechanik und Handhabung des Targetrades" - ICANS - IV Paper and Jül.Spez. 113/KFK., 1980

2. Bauer, G. - "The General Concept for a Spallation Neutron Source in the federal Republic of Germany" - Atomkernenergie/ Kerntechnik, in print, 1982

3. "Die Lösung der stationären und instationären Temperaturfeldgleichung für Ebene und räumliche Körper mittels der Finite-Element-Methode" - Manuscript for a Seminar at "Haus der Technik" in Essen, Book under preparation, Essen, 1981

4. Stelzer, F. - "Behaviour of the Spallation Neutron Source Target Wheelunder Thermaland Mechanical Loads" - Atomkernenergie/ Kerntechnik, to be published in Dec. 1982

5. ASTM. "Manual on the Use of Thermocouples in Temperature Measurement". Chap. 9. On Installation effects, ASTM. Special Technical Publication. STP 470 A Baltimore, 1974

6. Chapman, A.J. "Heat Transfer", Mac. Millan Publ. Co., New York, 1974

7. Zukauskas, A.A. "Heat Transfer of Banks of Tubes in Crossflow at High Reynolds Numbers" - Heat Exchangers: Design and Theory Source Book, Chap 4, Afgan, N.H. and Schlünder, E. U. Editors, McGraw-Hill, New York, 1974

8. Stelzer, F. - "Bedienungsanleitung und Programmbeschreibung für FEMFAM T"- Internal publication at ZAT - ZAT of the KFA-Jülich, Jülich, 1981

APPENDIX I

tables

Table 1. Characteristics of the System

- Channel	
h - 106 mm	height
w - 100 mm	wide
l - 290 mm	lenght
A - 4 x 1 x 106 = 424 mm^2	area of free flow
- Pin (Graphit)	
d - 24 mm	diameter
p - 25 mm	pitch
b - 20,8 mm	distance between 2 rows
p/d - 1,042	
e - 7 mm	thickness
l - 106 mm	lenght
w - 8,5 kw	total heat generated
- Thermocouples	
Type k	
Ø - 0,5 mm (pin)	diameter
Ø - 1,5 mm (in/outlet)	diameter
- Equipments	
Flowmeter (max. 6,5 m^3/h)	Krohne
Multipenrecorder (3)	Rikadenki
Digital Multimeter (2)	Keytley

Tabele 2 - Parameters for the experiment

flowrate - m^3/h

4,5; 4,0; 3,5; 3,0; 2,5

flowrate per pin in each row - m^3/h

1,125; 1,0; 0,875; 0,750; 0,625

Electrical current - A

100, 200, ..., 800, 850

Angles-

0^o, 30^o, 60^o, 90^o, 120^o, 150^o, 180^o

Table 3 Overtemperatures as function of θ

Re	W	0°	30°	60°	90°	120°	150°	180°	Nu
71256	121,0	0,13	0,97	1,08	1,46	1,41	1,78	0,71	559,2
		0,24	1,09	1,20	1,76	1,51	1,86	0,85	995,0
63455	121,0	0,17	1,02	1,22	1,56	1,56	1,88	0,73	516,3
		0,29	1,14	1,34	1,85	1,66	1,96	0,89	440,9
55366	121,0	0,25	1,15	1,36	1,74	1,69	2,06	0,97	457,7
		0,37	1,27	1,47	1,98	1,79	2,14	1,11	416,7
47598	121,0	0,28	1,28	1,43	1,82	1,86	2,19	1,13	422,6
		0,40	1,40	1,55	2,06	1,96	2,27	1,26	387,4
39616	121,0	0,34	1,39	1,53	1,93	1,97	2,40	1,26	389,9
		0,46	1,51	1,65	2,12	2,07	2,48	1,40	361,9

Table 4 Overtemperatures as function of θ

Re	W	0°	30°	60°	90°	120°	150°	180°	Nu
71166	483,0	3,67	4,85	5,58	5,62	5,81	6,77	5,23	451,1
		4,10	5,34	6,05	6,37	6,21	7,16	5,78	412,6
63219	482,8	3,89	5,08	5,81	6,07	6,19	7,11	5,18	430,2
		4,33	5,57	6,29	6,59	6,59	7,50	6,26	392,5
55281	982,6	4,17	5,31	6,04	6,33	6,58	7,54	6,06	402,9
		4,61	5,80	6,51	7,08	6,97	7,92	6,58	371,9
47587	482,3	6,62	5,62	6,45	6,79	7,14	7,95	7,03	355,5
		7,02	6,11	6,92	7,54	7,54	8,34	7,56	331,6
39616	482,1	4,83	6,22	6,89	7,29	7,62	9,05	7,14	344,8
		5,27	6,70	7,36	8,03	8,02	9,43	7,69	322,3

Table 5 Overtemperatures as function of θ

Re	W	0°	30°	60°	90°	120°	150°	180°	Nu
71197	1070	9,01	10,95	12,24	12,37	12,72	14,58	11,66	448,5
		9,95	12,02	13,28	13,61	13,61	15,44	12,87	412,5
63261	1069	9,58	11,41	12,90	12,99	13,44	15,44	12,52	439,2
		10,52	12,48	13,95	14,42	14,32	16,31	13,73	391,0
55390	1068	9,87	11,91	13,36	13,79	14,09	16,04	13,43	404,9
		10,83	12,99	14,40	14,84	14,98	16,90	14,63	376,1
47629	1067	10,63	12,81	14,20	14,89	15,13	17,33	14,66	374,2
		11,59	13,88	15,25	16,02	16,02	18,19	15,87	349,2
39668	1065	11,53	13,66	15,21	15,74	16,25	18,38	16,00	349,4
		12,49	14,74	16,26	17,02	17,13	19,25	16,82	327,7

Table 6 Overtemperatures as function of θ

Re	W	0°	30°	60°	90°	120°	150°	180°	Nu
71401	1865	16,24	18,90	20,84	21,02	24,63	24,37	19,70	457,5
		17,89	20,78	22,68	23,44	23,19	25,90	21,84	419,3
63455	1862	17,09	19,49	21,89	22,03	22,77	25,30	20,89	436,0
		18,74	21,37	23,72	24,93	24,33	26,83	23,03	399,8
55499	1860	17,64	20,00	22,71	23,21	24,05	26,36	22,32	415,9
		19,30	21,88	24,56	25,81	25,61	27,88	24,46	383,6
47796	1858	18,56	20,86	24,07	24,10	25,66	27,79	23,84	394,3
		20,22	22,75	25,91	27,22	27,21	29,32	25,98	363,9
39860	1854	19,73	21,95	25,31	26,18	27,52	30,16	26,21	366,3
		21,40	23,83	27,16	28,79	29,08	31,68	28,34	340,8

Table 7 — Overtemperatures as function of θ

Re	W	0°	30°	60°	90°	120°	150°	180°	Nu
71604	2893	25,26	28,01	31,38	32,02	32,52	48,25	30,03	436,8
		27,79	30,89	34,21	34,97	34,60	50,40	33,32	403,6
63678	2838	26,14	28,58	32,87	34,60	34,60	49,96	31,14	420,1
		28,68	31,46	35,75	36,98	36,99	52,11	34,45	387,0
55718	2833	27,39	29,74	34,25	34,33	36,40	51,25	31,47	404,5
		29,96	32,64	37,09	38,40	38,79	53,41	35,80	372,3
48027	2828	28,97	31,09	36,47	36,65	38,82	53,57	34,91	379,6
		31,55	33,99	39,27	40,26	41,19	55,73	38,24	352,9
40078	2819	30,64	32,98	38,01	39,06	41,10	56,06	38,30	356,4
		33,24	35,90	40,80	42,95	43,97	58,22	41,63	332,3

Table 8 Overtemperatures as function of θ

Re	W	0°	30°	60°	90°	120°	150°	180°	Nu
72123	3989	35,06	39,98	43,03	43,42	44,59	48,61	40,07	472,9
		38,63	44,04	47,05	48,06	48,01	51,97	44,75	432,3
64083	3979	36,57	40,37	44,35	45,02	47,17	50,89	44,07	450,6
		40,17	44,46	48,38	50,44	50,59	54,26	48,73	412,3
56060	3966	37,62	42,62	46,28	97,21	99,36	55,16	54,02	416,9
		41,21	46,70	50,32	51,24	52,78	58,50	58,58	384,0
48290	3949	38,11	45,55	49,19	50,05	52,73	61,08	62,48	383,7
		41,73	49,63	53,21	55,11	56,13	64,39	66,96	356,0
40288	3932	42,01	47,98	51,92	54,32	56,34	64,53	67,09	358,6
		45,62	51,57	55,95	58,78	59,75	67,84	71,57	333,8

Table 9

Overtemperatures as function of θ

Re	W	0°	30°	60°	90°	120°	150°	180°	Nu
72454	5261	46,92	51,38	56,05	56,48	58,45	62,27	55,52	474,6
		51,73	56,87	61,47	62,43	63,06	66,83	61,79	433,1
64503	5240	48,25	52,94	58,36	58,77	61,18	65,04	63,93	446,8
		53,78	58,44	63,75	65,01	65,79	69,6	70,17	409,4
56452	5222	50,68	55,49	61,48	61,84	63,62	69,89	66,19	424,6
		55,51	61,01	66,90	67,27	68,23	73,72	72,47	391,8
48712	5198	52,56	58,33	64,35	64,48	66,54	77,35	69,90	399,8
		57,41	63,82	69,78	71,13	71,16	81,85	76,19	369,0
40737	5173	55,85	61,77	68,97	68,85	68,64	81,69	73,20	379,1
		60,69	67,28	74,37	74,52	73,29	85,93	79,50	349,8

Table 10 Overtemperatures as function of θ

Re	W	0°	30°	60°	90°	120°	150°	180°	Nu
72944	6663	56,12	66,03	67,45	65,29	66,35	77,53	64,19	499,6
		62,32	73,06	74,49	75,99	72,41	83,41	72,38	452,3
64827	6636	57,88	68,04	68,76	68,31	68,87	79,73	72,62	477,7
		64,09	75,09	75,85	77,70	74,65	85,65	80,72	432,2
56735	6613	59,87	69,76	70,22	70,33	70,83	82,96	77,25	460,0
		66,08	76,82	77,33	78,69	76,92	88,86	85,32	419,2
48934	6578	63,11	73,94	72,11	74,05	75,00	87,63	83,77	432,8
		68,95	80,99	79,24	81,44	81,26	93,53	91,83	397,1
40941	6544	66,48	78,03	74,75	76,72	79,20	93,15	92,09	406,5
		72,72	85,08	81,91	84,15	85,28	98,99	98,00	375,9

Table 11 Overtemperatures as function of θ

Re	W	0°	30°	60°	90°	120°	150°	180°	Nu
73246	7372	64,33	70,31	72,00	70,22	71,97	82,27	76,32	506,2
		71,29	78,25	79,96	81,12	78,79	88,92	85,41	455,7
65207	7342	67,23	72,30	73,44	73,32	75,64	84,92	80,96	484,7
		74,20	80,27	82,43	82,94	82,46	91,61	90,06	438,1
57130	7316	68,88	73,32	74,26	76,59	78,41	86,94	85,42	468,4
		75,88	81,31	82,30	85,01	85,26	93,63	94,51	426,1
49360	7280	71,20	77,89	77,43	79,82	81,49	90,83	91,55	444,3
		78,22	85,87	85,43	87,86	88,33	97,53	100,56	406,1
41322	7236	73,68	85,14	80,53	83,24	85,00	95,62	97,84	418,7
		80,72	93,06	88,57	91,29	91,84	102,31	106,85	384,3

Table 12 Local heat transfer coefficient - $\alpha_\theta/\bar{\alpha}$

Re	0°	30°	60°	90°	120°	150°	180°
73246	1,129	1,030	1,007	1,013	0,952	0,957	0,947
62207	1,123	1,041	1,020	1,017	1,005	0,900	0,929
57130	1,127	1,055	1,042	1,010	0,997	0,903	0,907
49360	1,142	1,043	1,048	1,018	1,005	0,906	0,888
41322	1,162	1,007	1,061	1,028	1,014	0,867	0,876

APPENDIX II

Figures

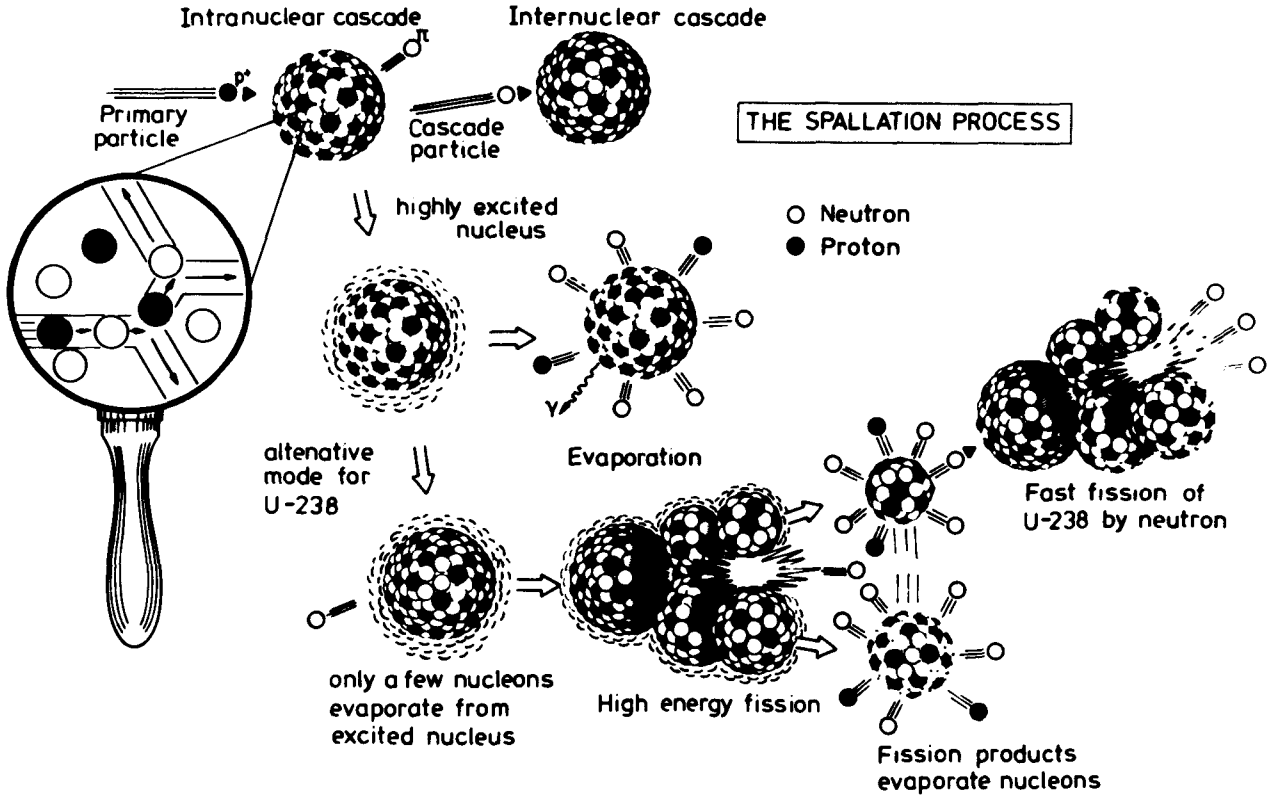

Fig. 1 Schematic description of the spallation process Ref. /2/.

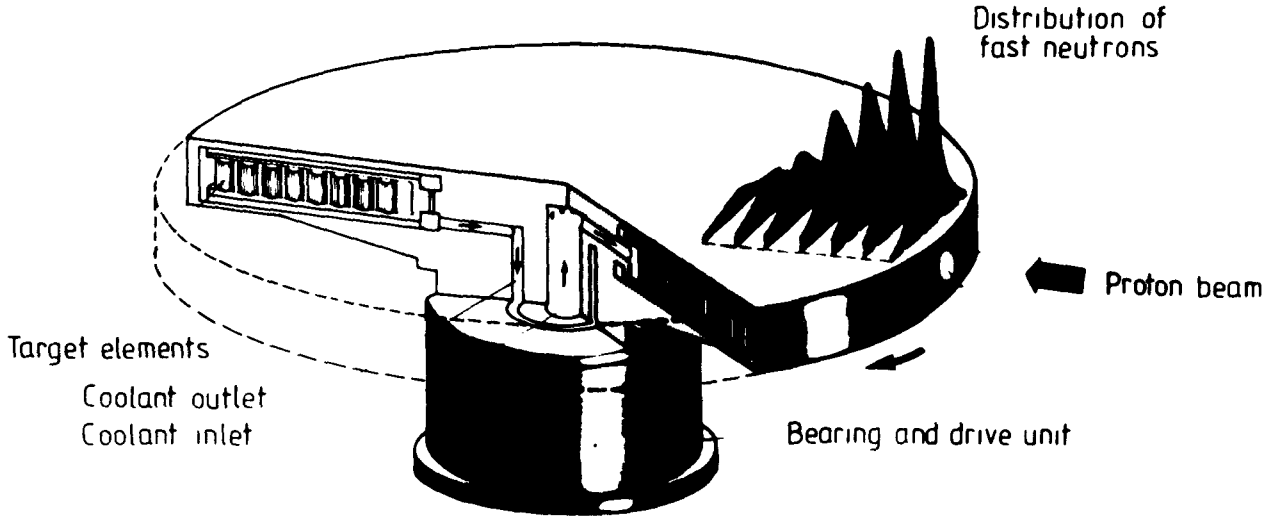

Fig. 2 Schematic Representation of the Target Wheel, showing the fast neutrons distribution and the local of incidence of the proton beam. The wheel rotates at 0,5 Hz.

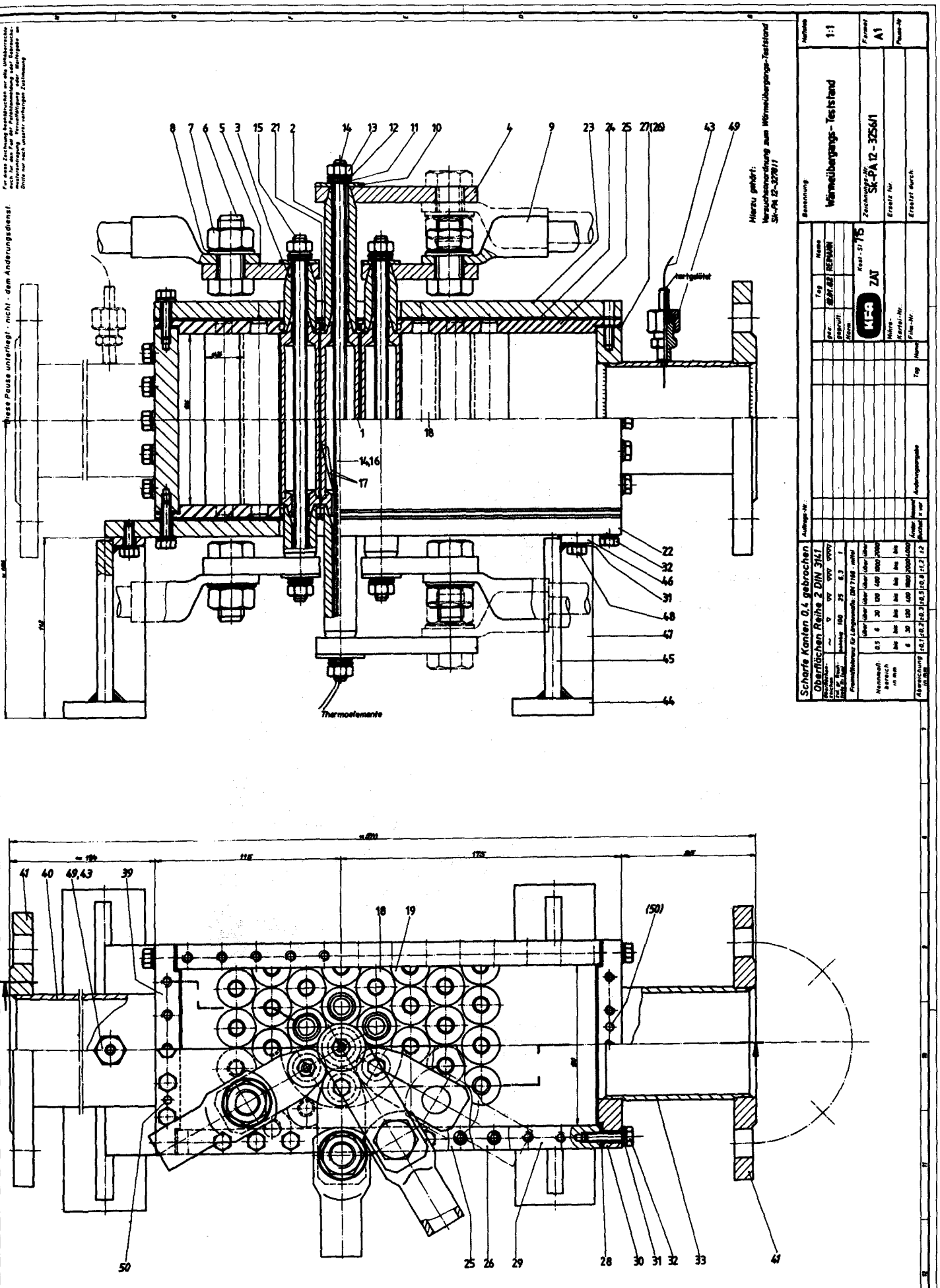

Fig. 3 The Test Apparatus

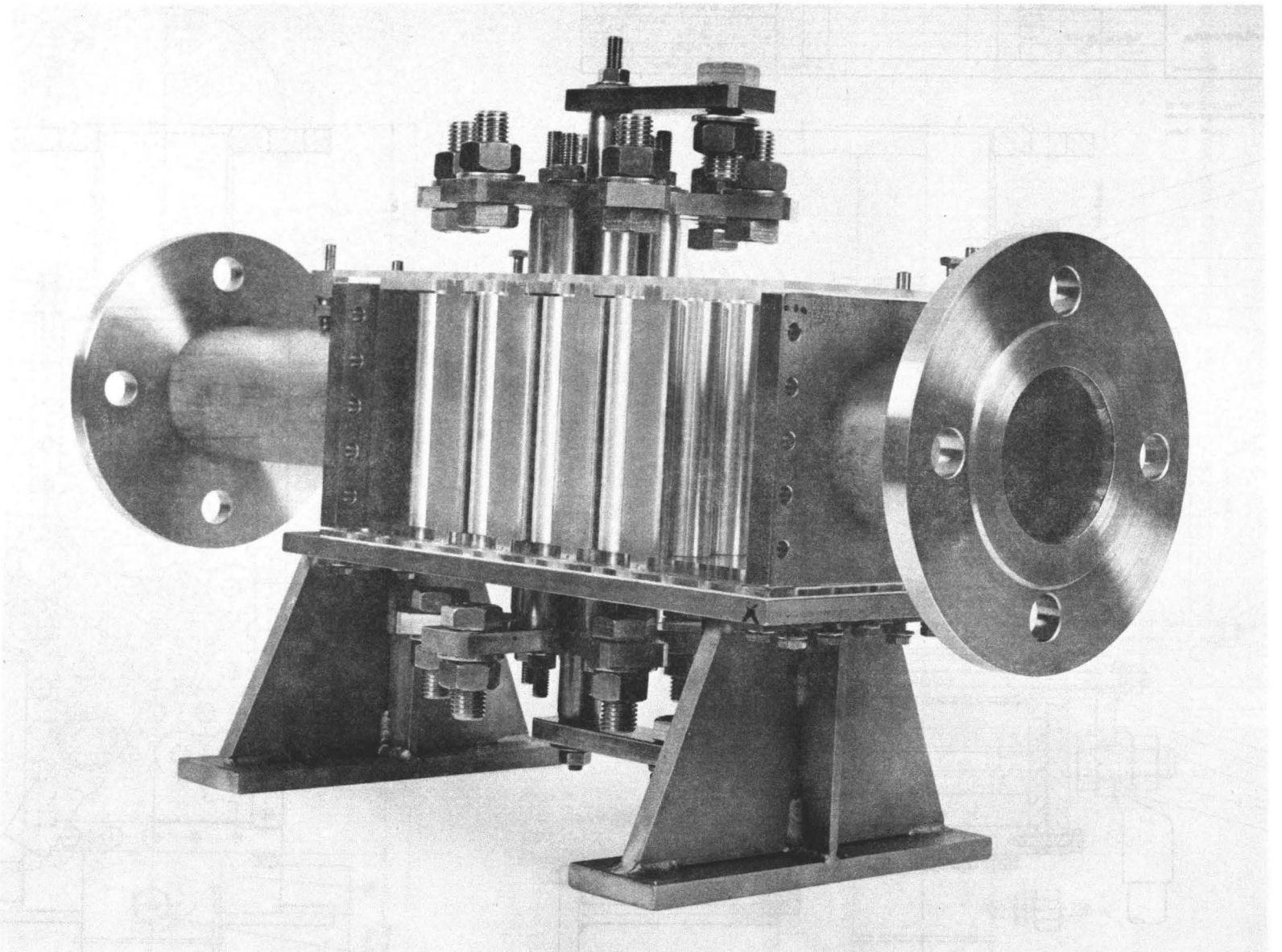

Fig. 4 View of the Test Apparatus, showing the pins, the plexiglass plates and the electrical contacts.

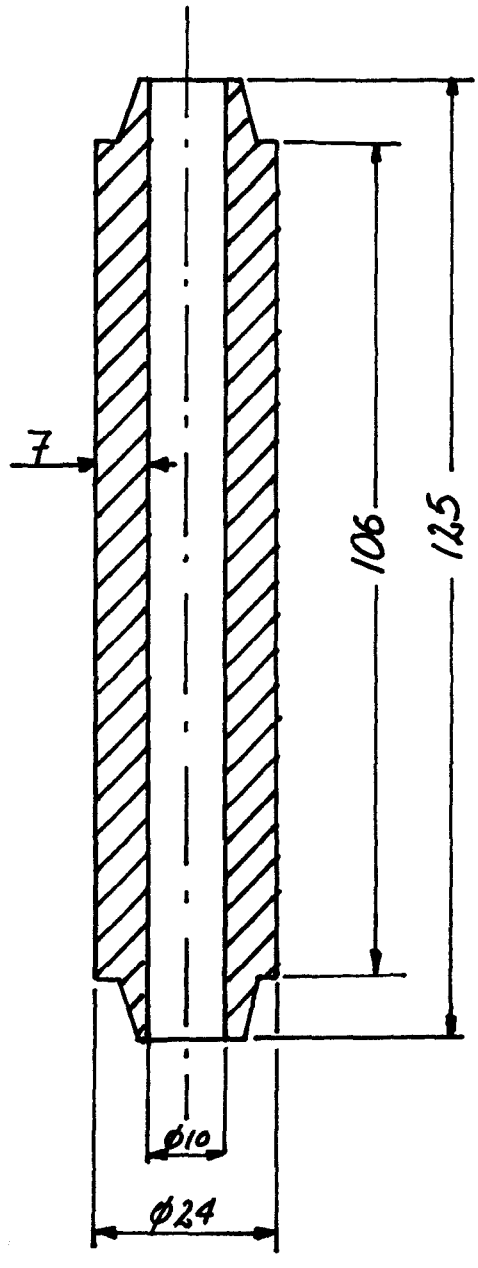

Fig. 5 The graphit pin - main dimensions.

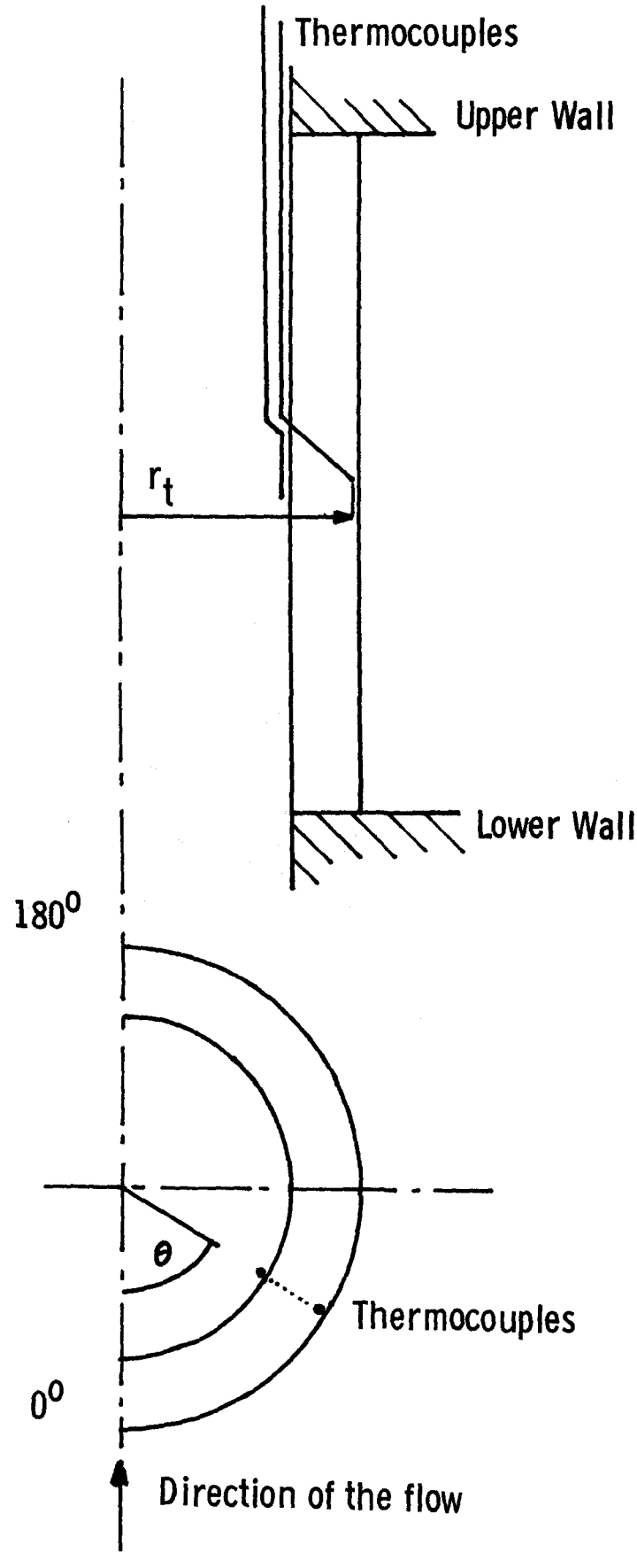

Fig. 6 Schematic representation of one pair of thermocouples inside pin.

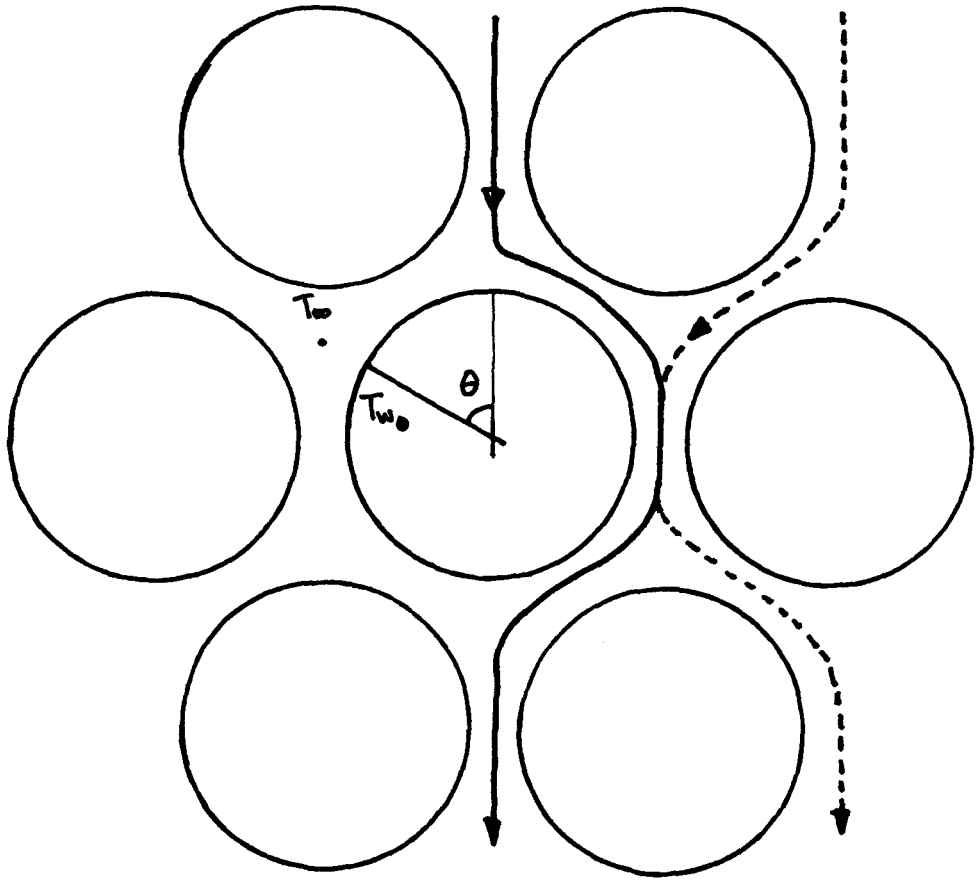

Main direction of the flow through the pins

Fig. 7 Schematic representation of the flow path across the pin bank.

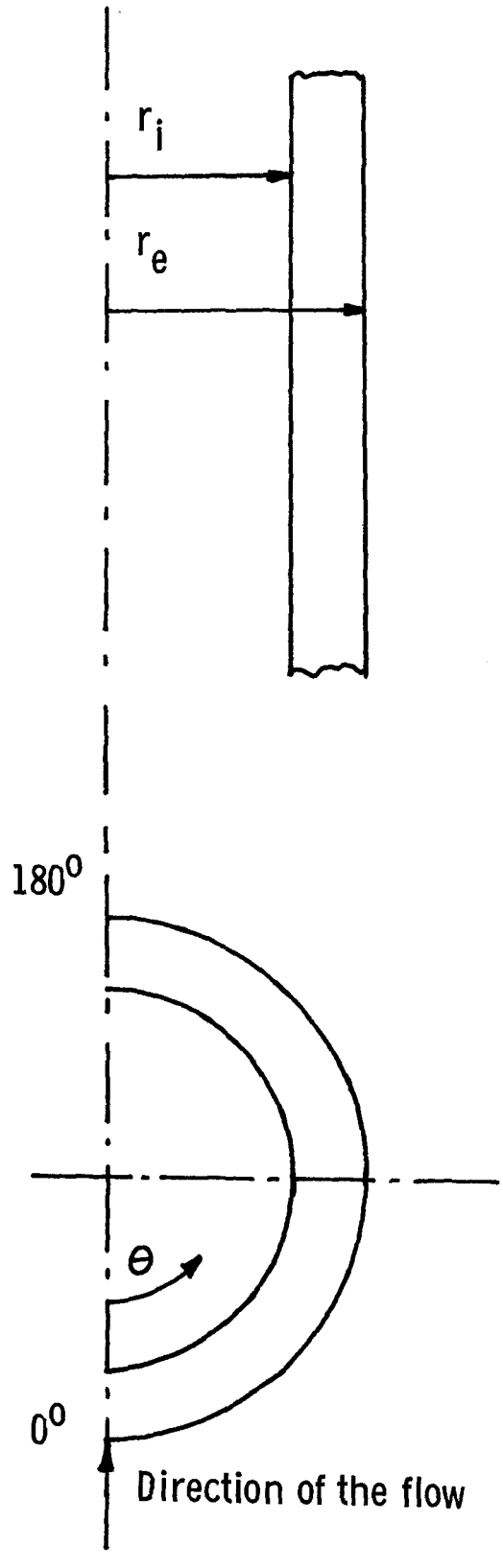

Fig. 8 Schematic representation of one pin, showing the coordinate system and the symbology adopted.

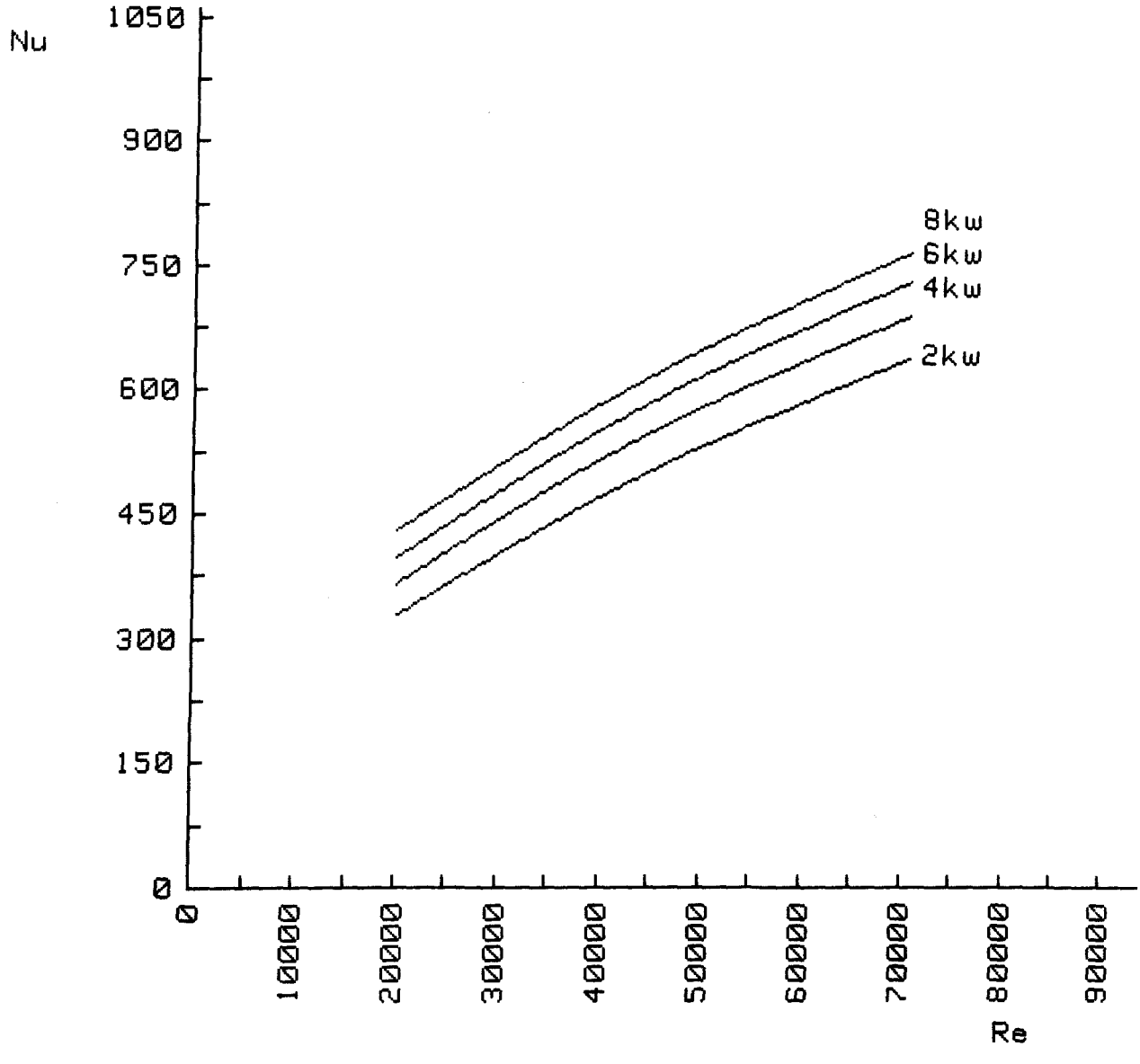

Fig. 9 Nusselt Number as a function of Reynolds Number, taking the heat production as parameter, calculated through Equations (8) and (9).

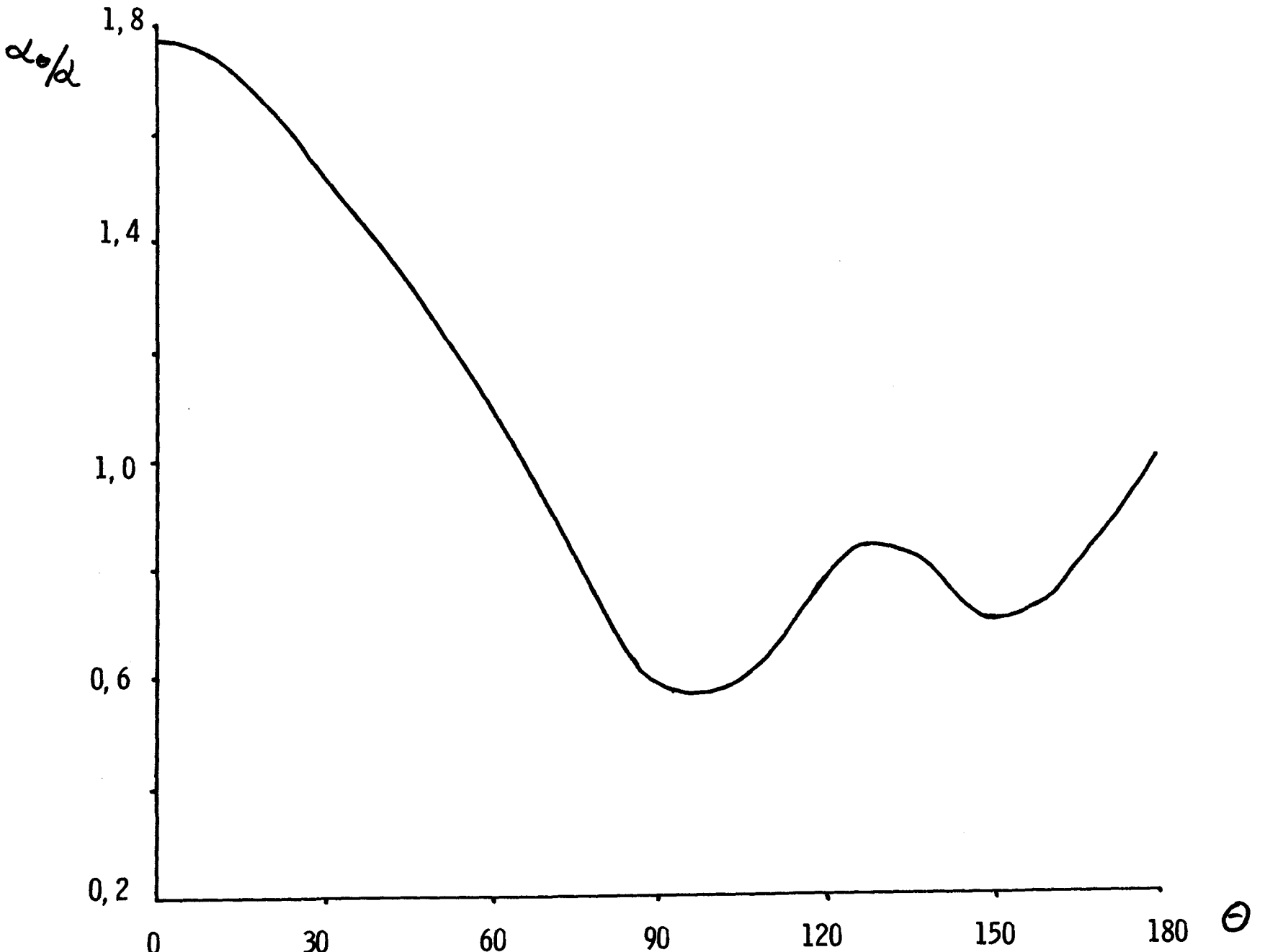

Fig. 10 Local heat transfer coefficient for a tube in a staggered bank Ref. /7/.

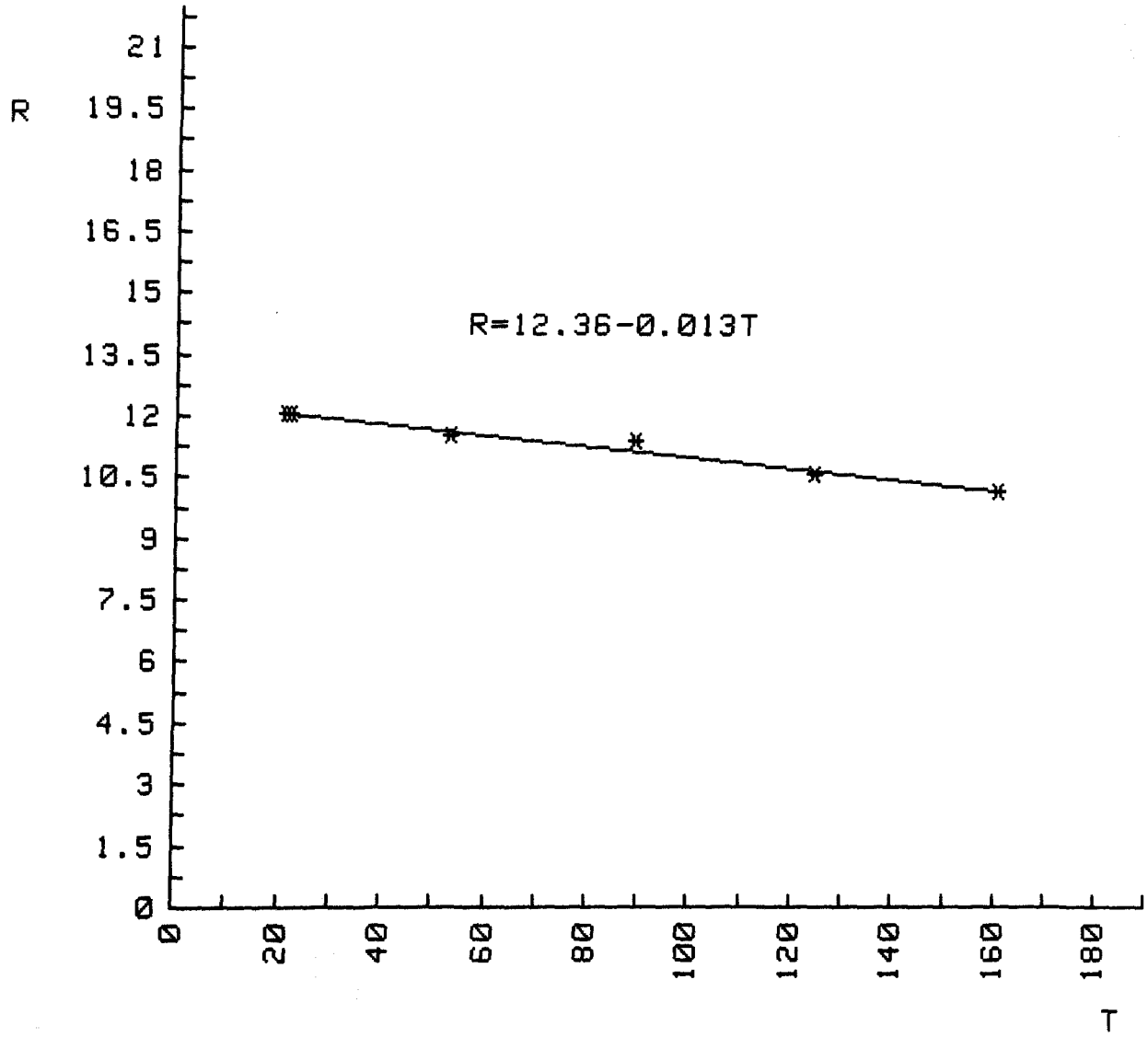

Fig. 11 Electrical Resistivity of the Graphit Pin (mΩ).

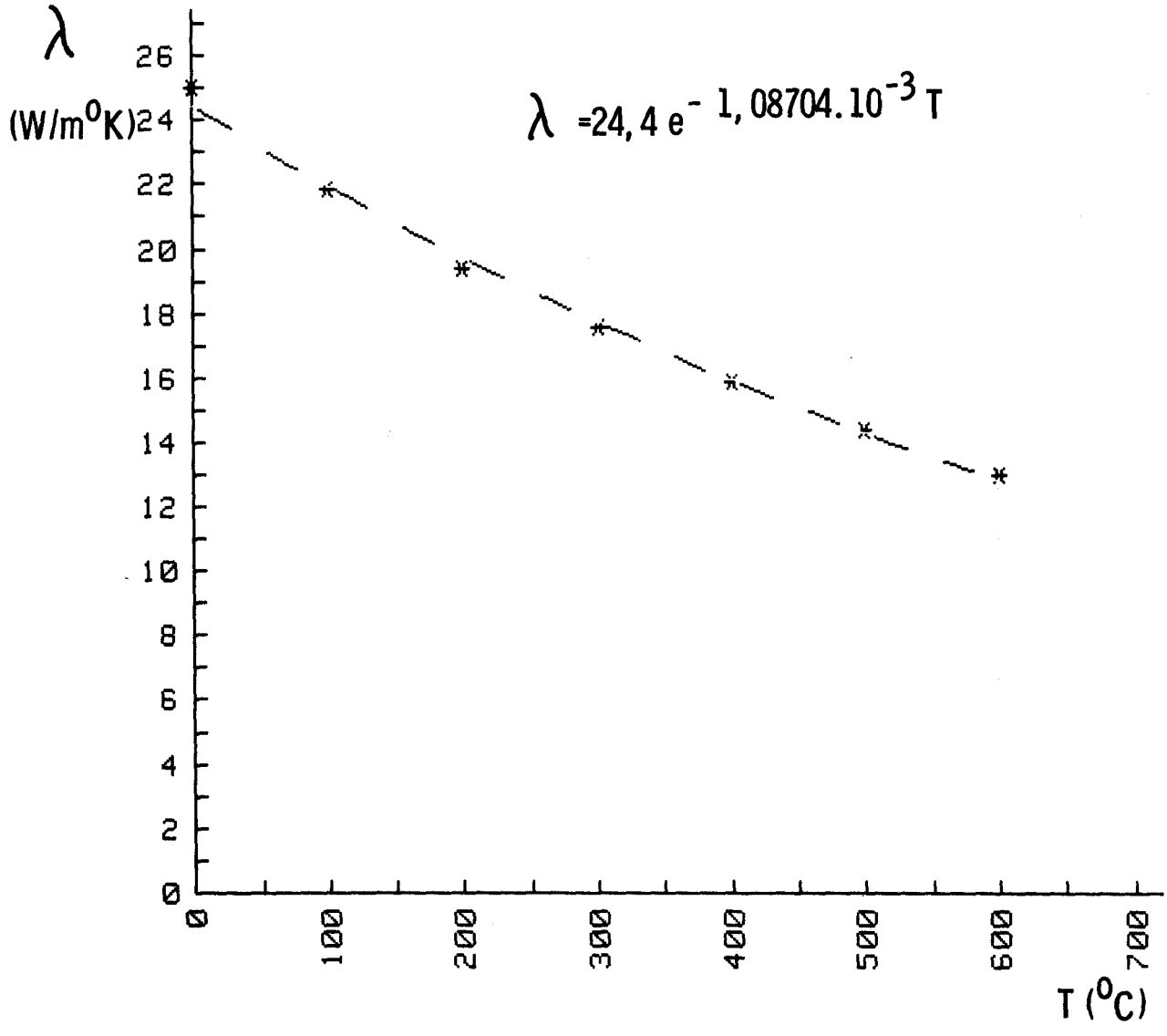

Fig. 12 Thermal Conductivity of Graphit.

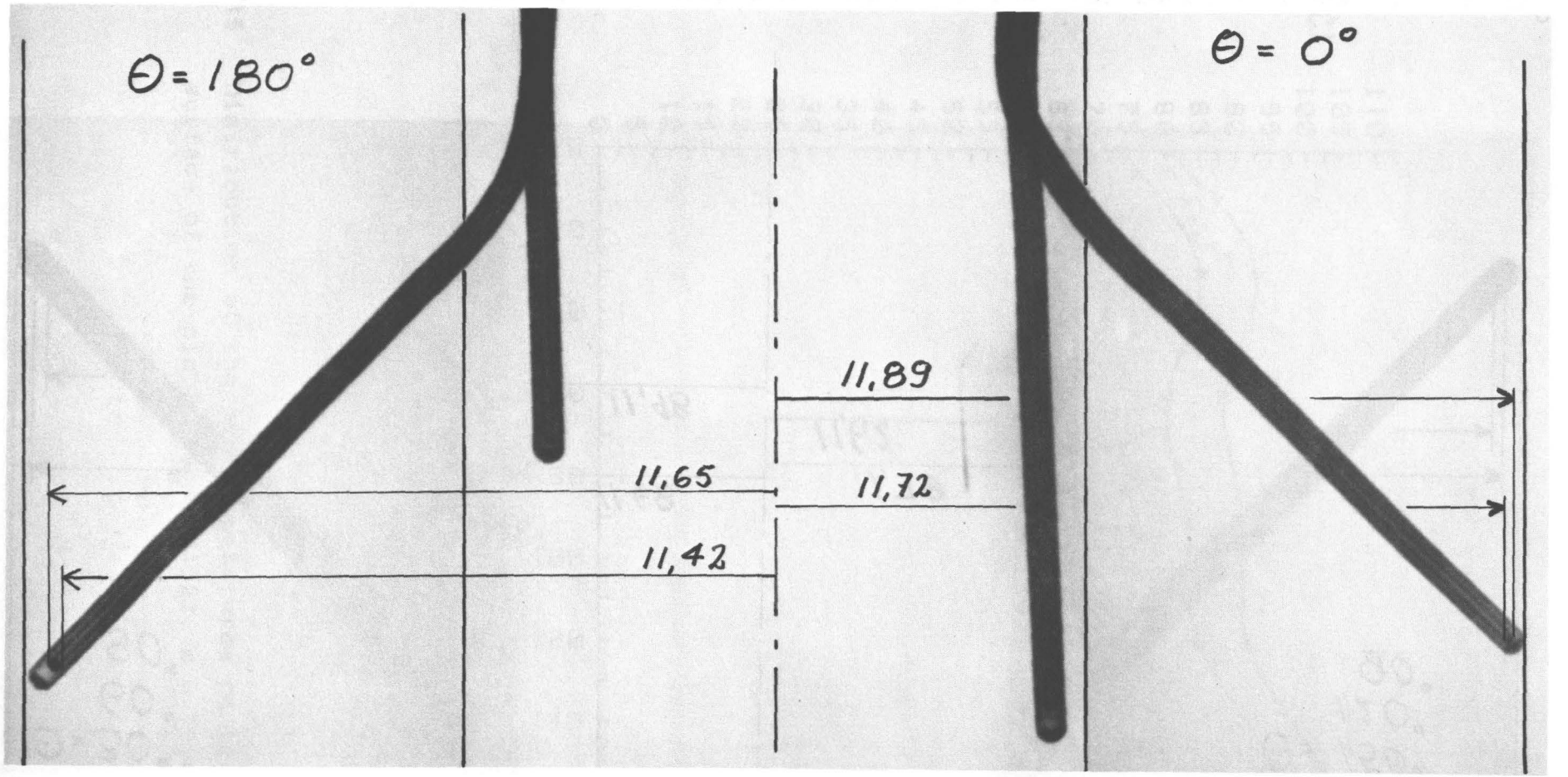

Fig. 13 Radiographic picture of the graphit pin used for the measurements at 0° and 180°, showing the values for r_t.

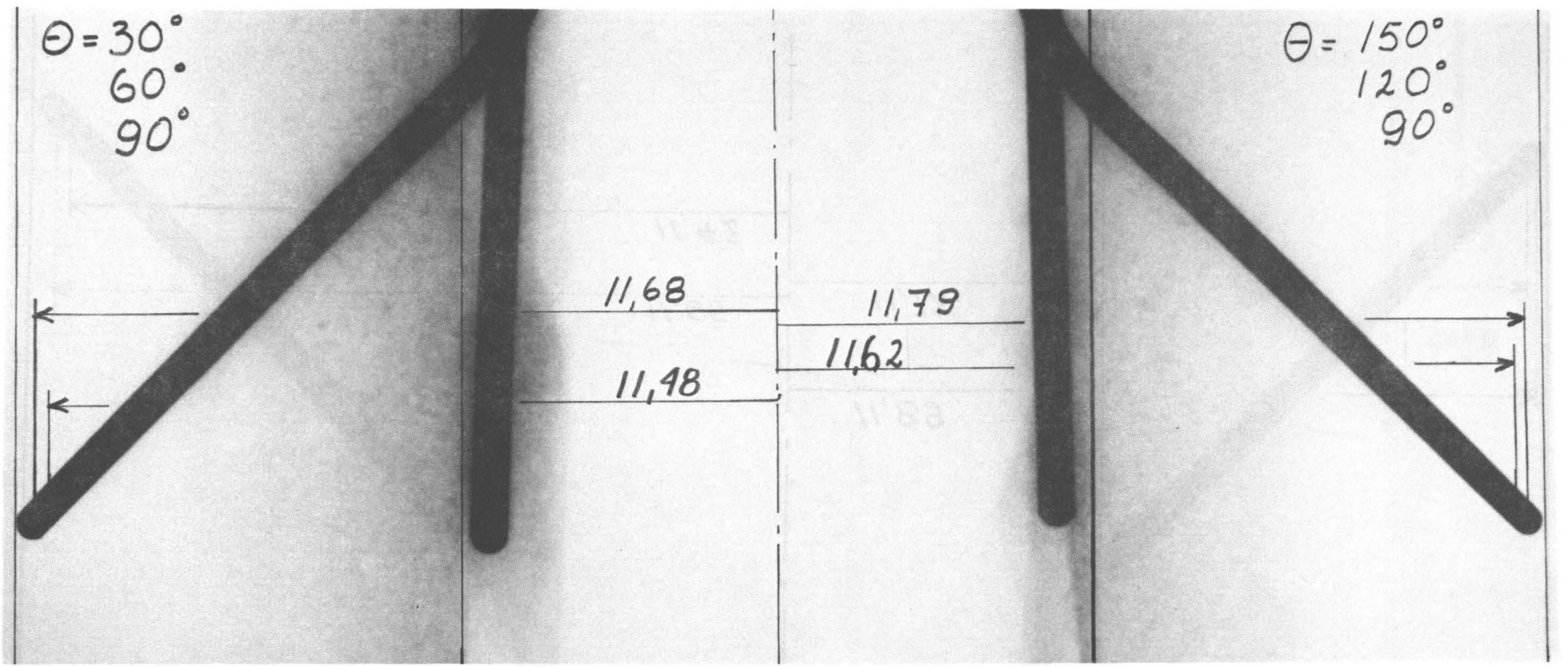

Fig. 14 Radiographic picture of the graphit pin used for the measurements at angles from 30° to 150°, showing the values for r_t.

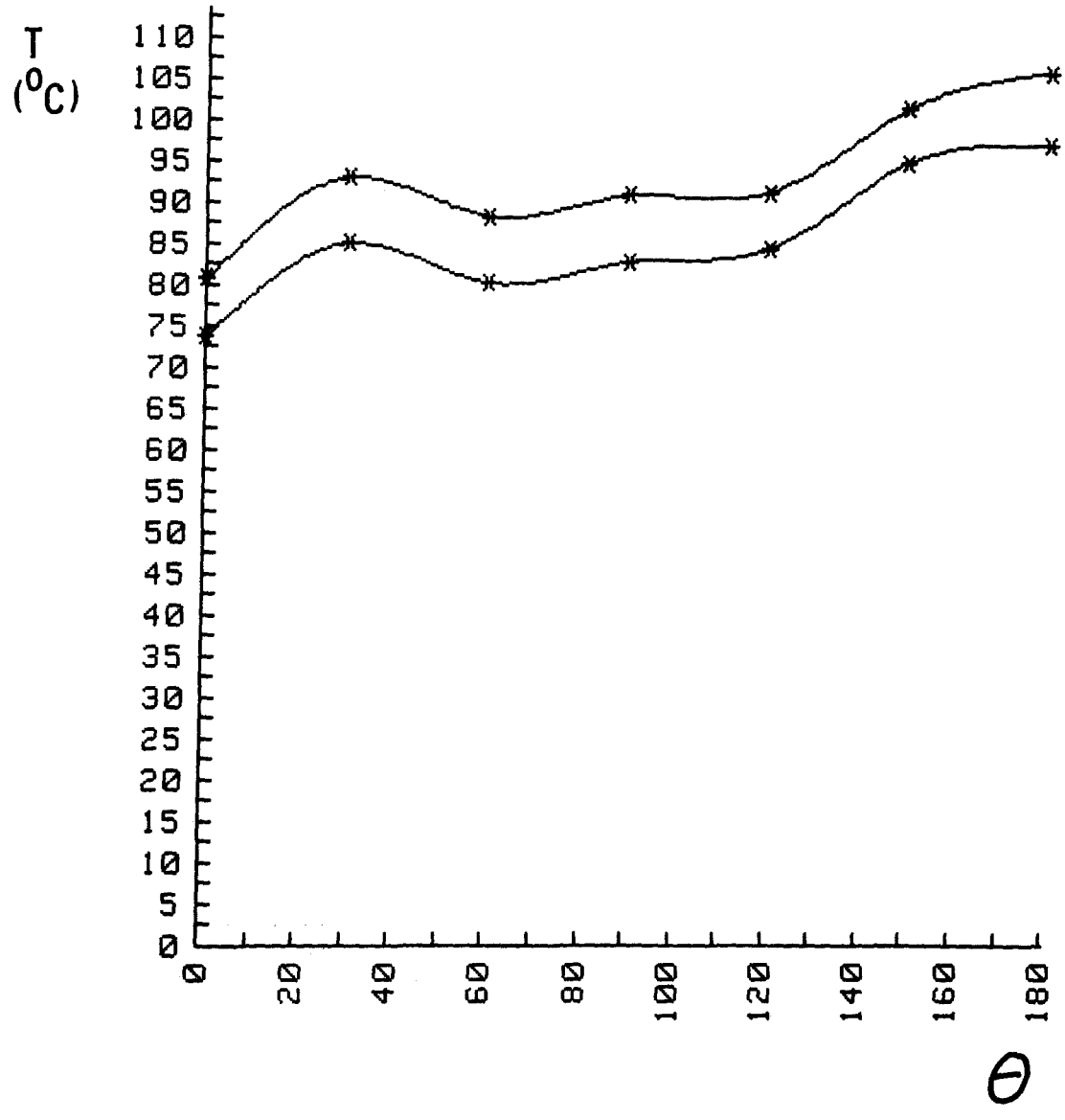

Fig. 15 Distribution of the overtemperatures on the external surface of the pin for R_e = 41322, W = 7236 W.

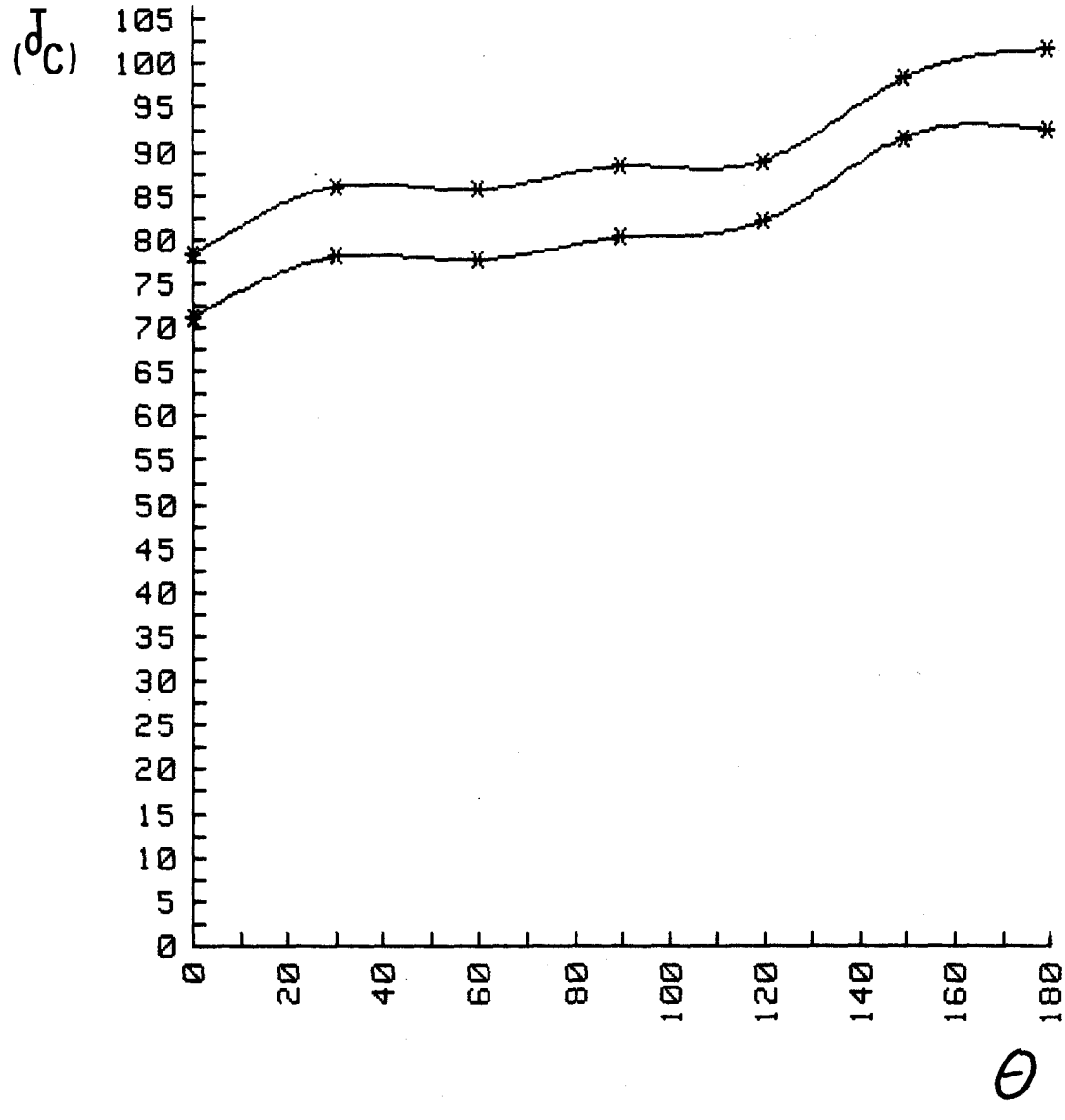

Fig. 16 Distribution of the overtemperatures on the external surface of the pin for Re = 49360, W = 7280 w.

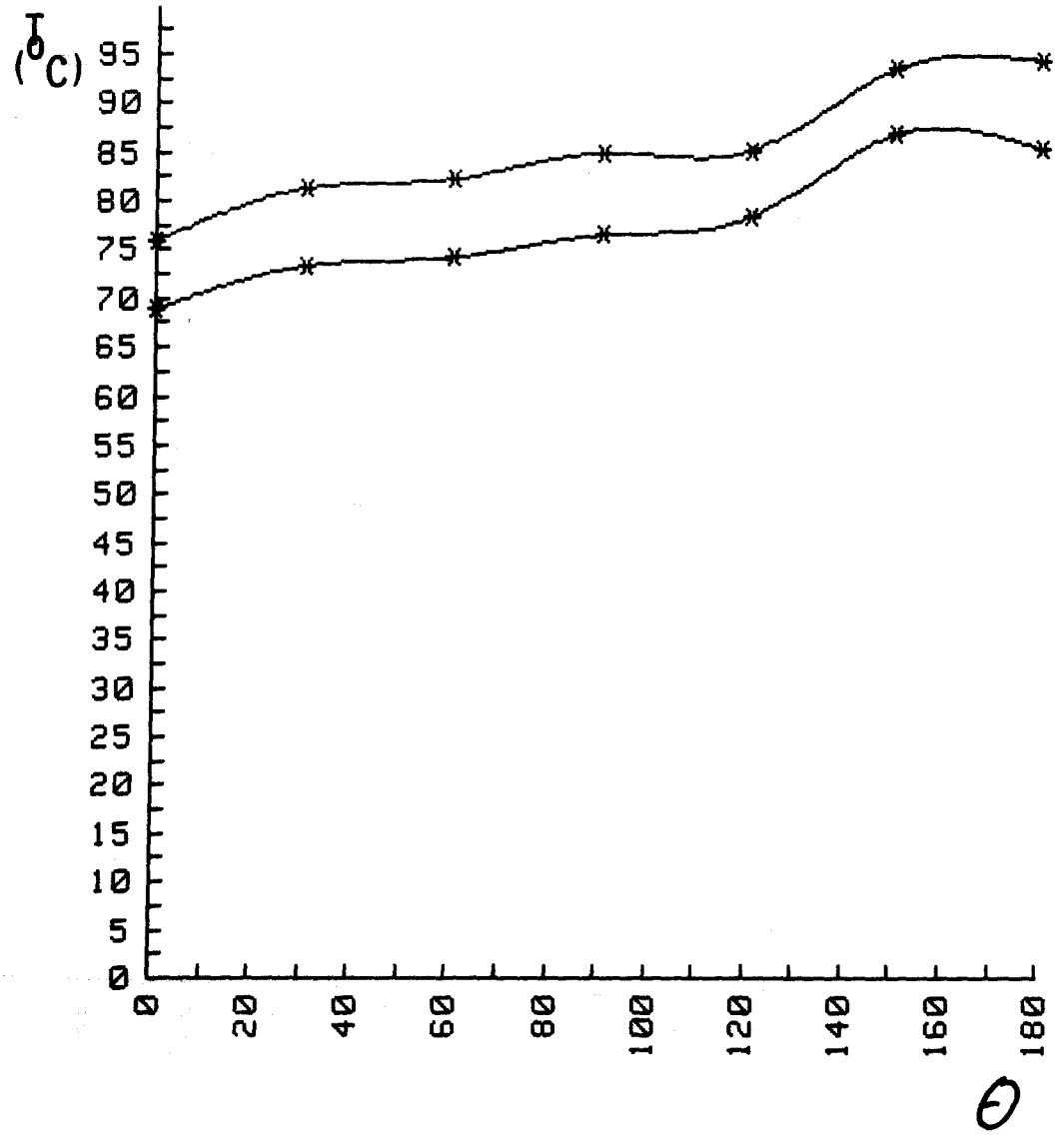

Fig. 17 Distribution of the overtemperatures on the external surface of the pin for Re = 57130, W = 7316 w.

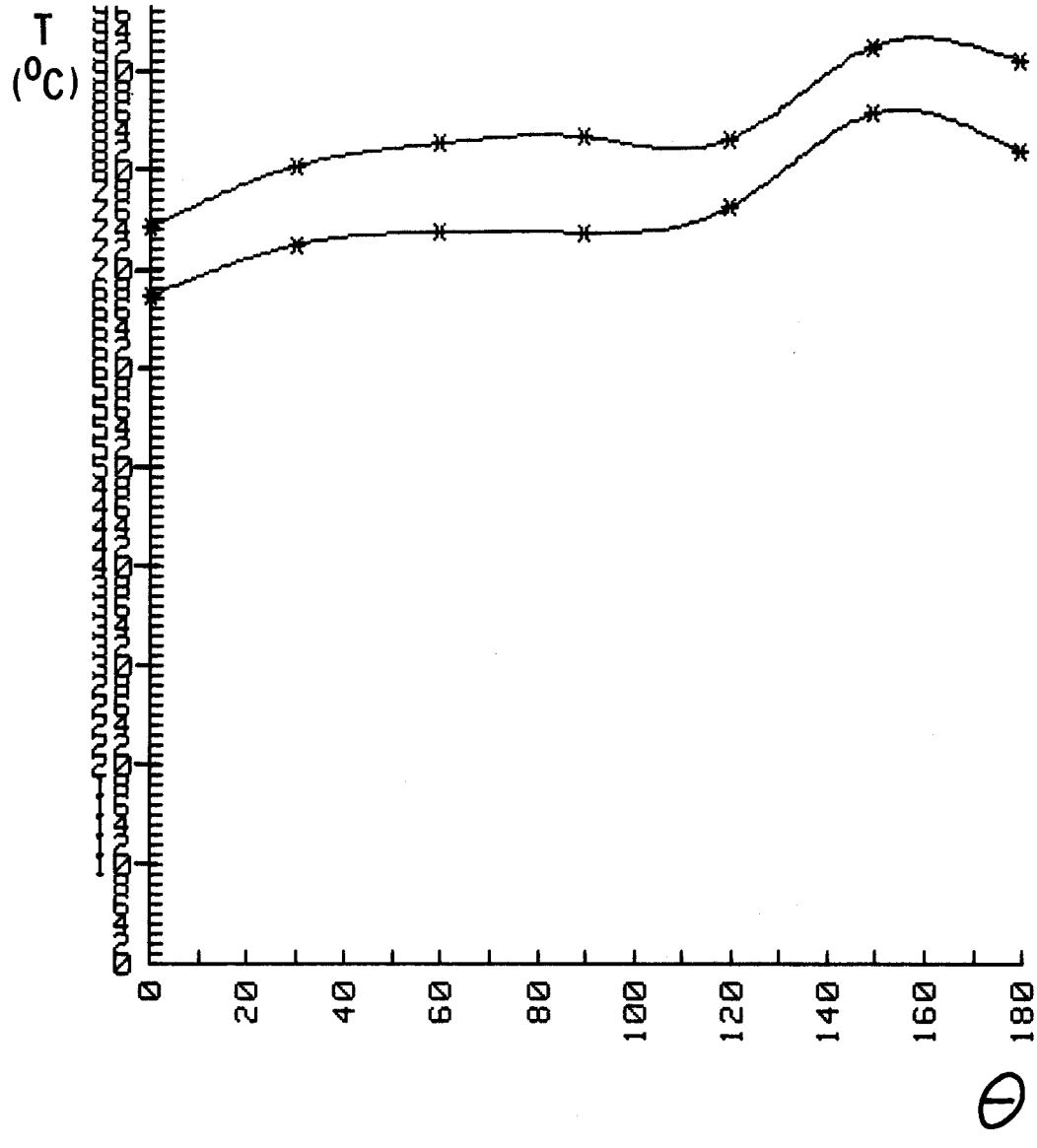

Fig. 18 Distribution of the overtemperatures on the external surface of the pin for Re = 65207, W = 7342 w.

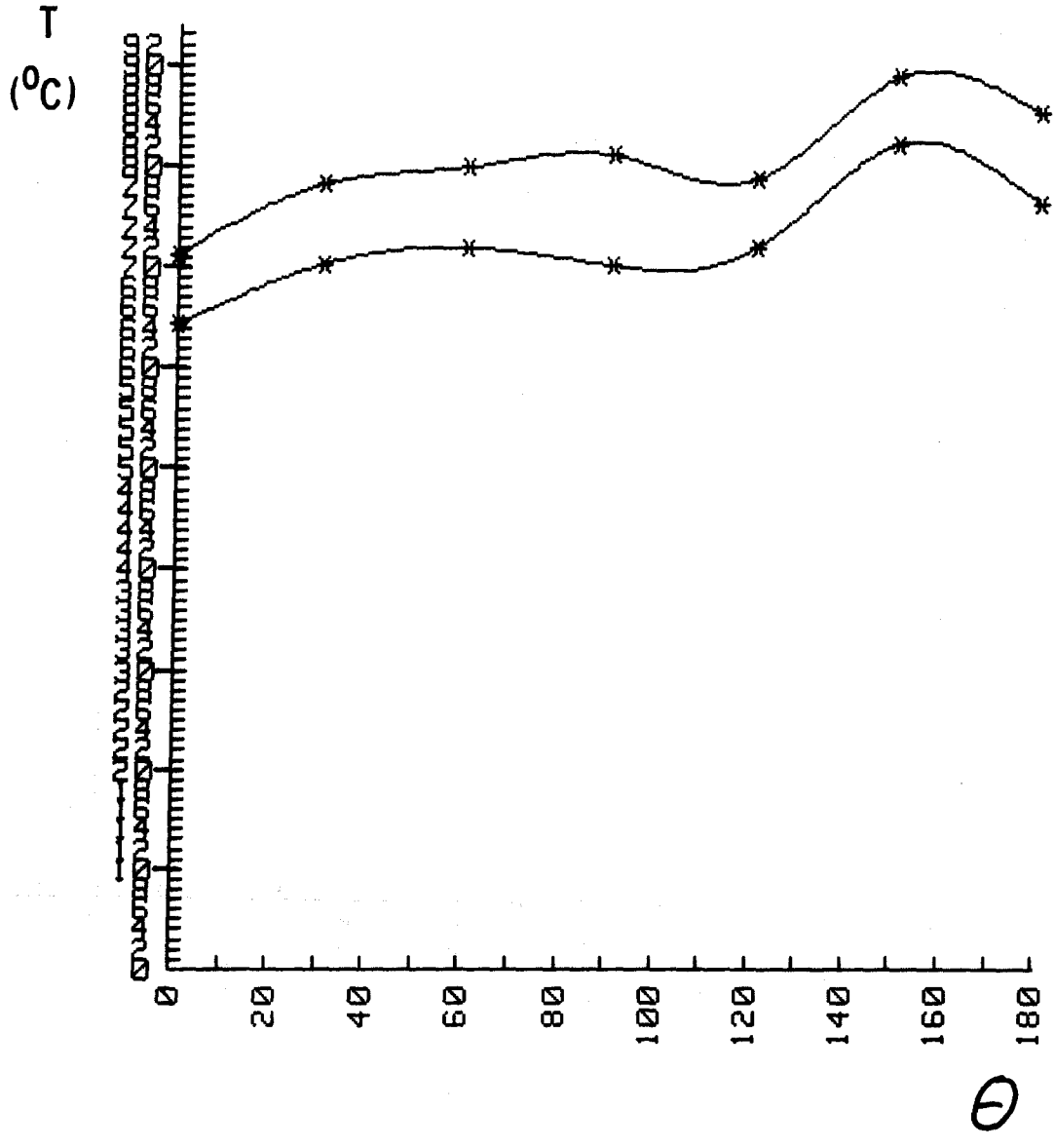

Fig. 19 Temperature distribution on the external surface of the pin for Re = 73246, W = 7372 w.

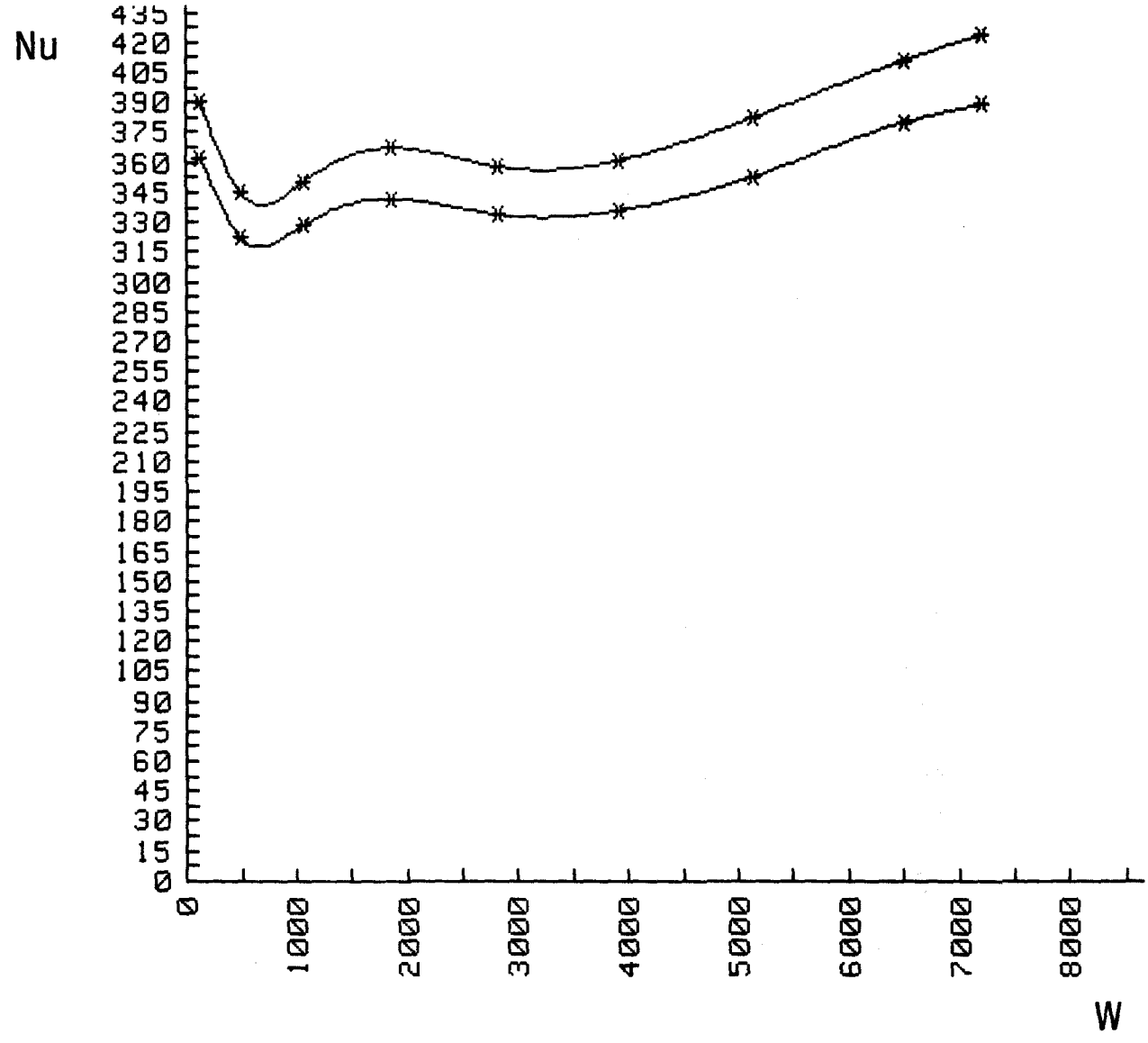

Fig. 20 Behaviour of the Nusselt Number as function of the heat production for an average Re = 40236 (s=631).

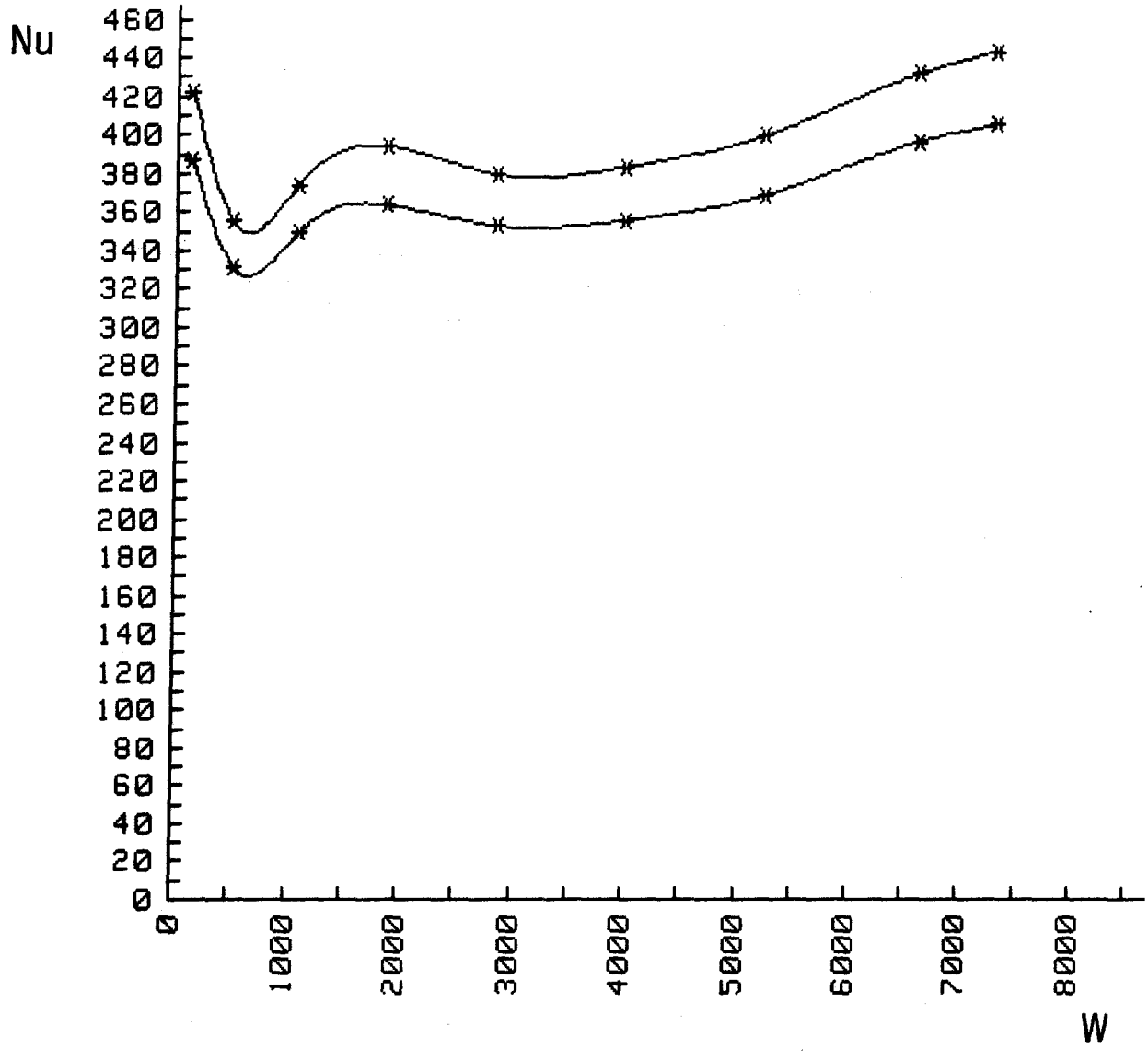

Fig. 21 Behaviour of the Nusselt Number as a function of the heat production for an average Re = 48215 (s=653)

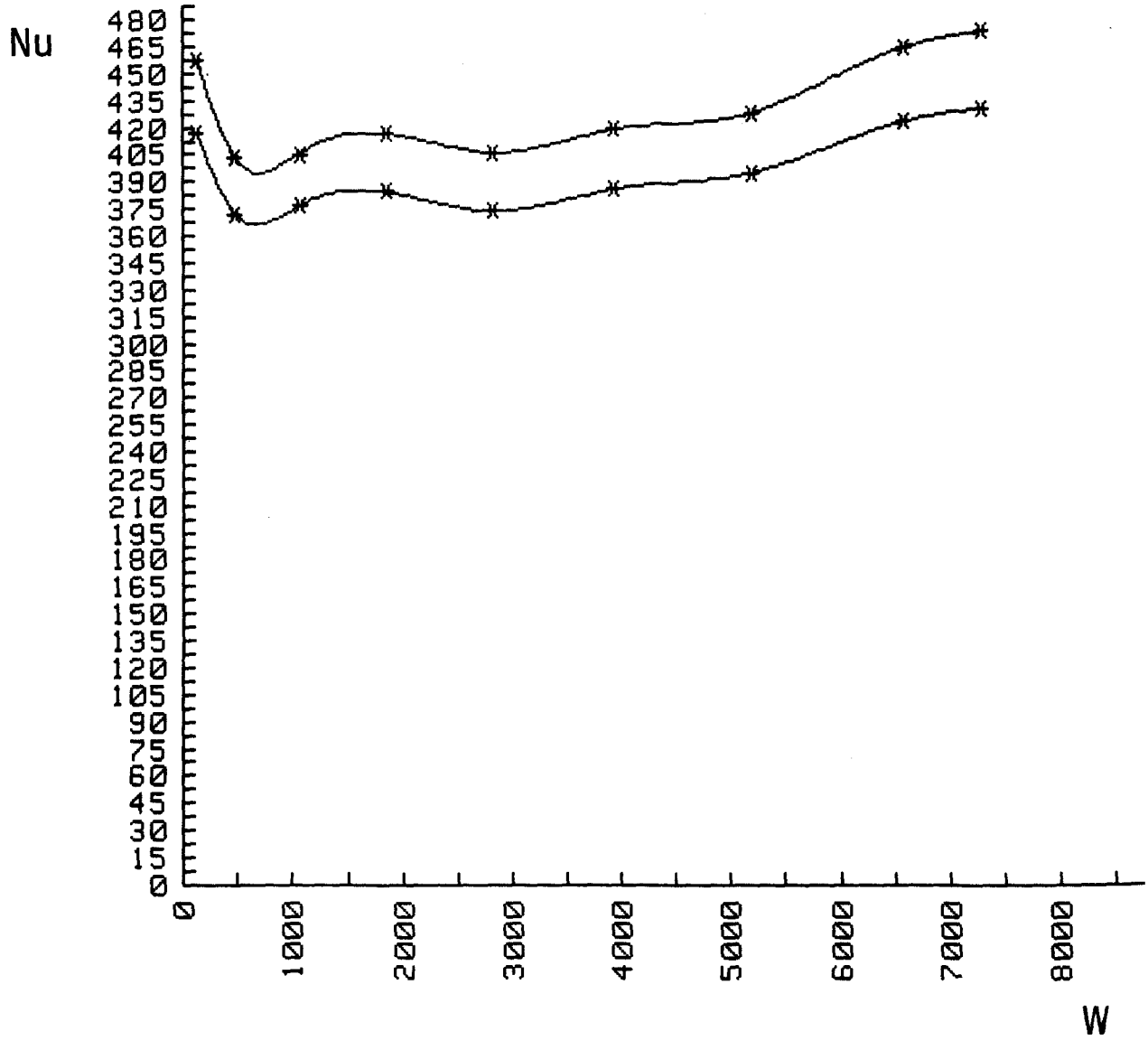

Fig. 22 Behaviour of the Nusselt Number as a function of the heat production for an average Re=55959 (s=674).

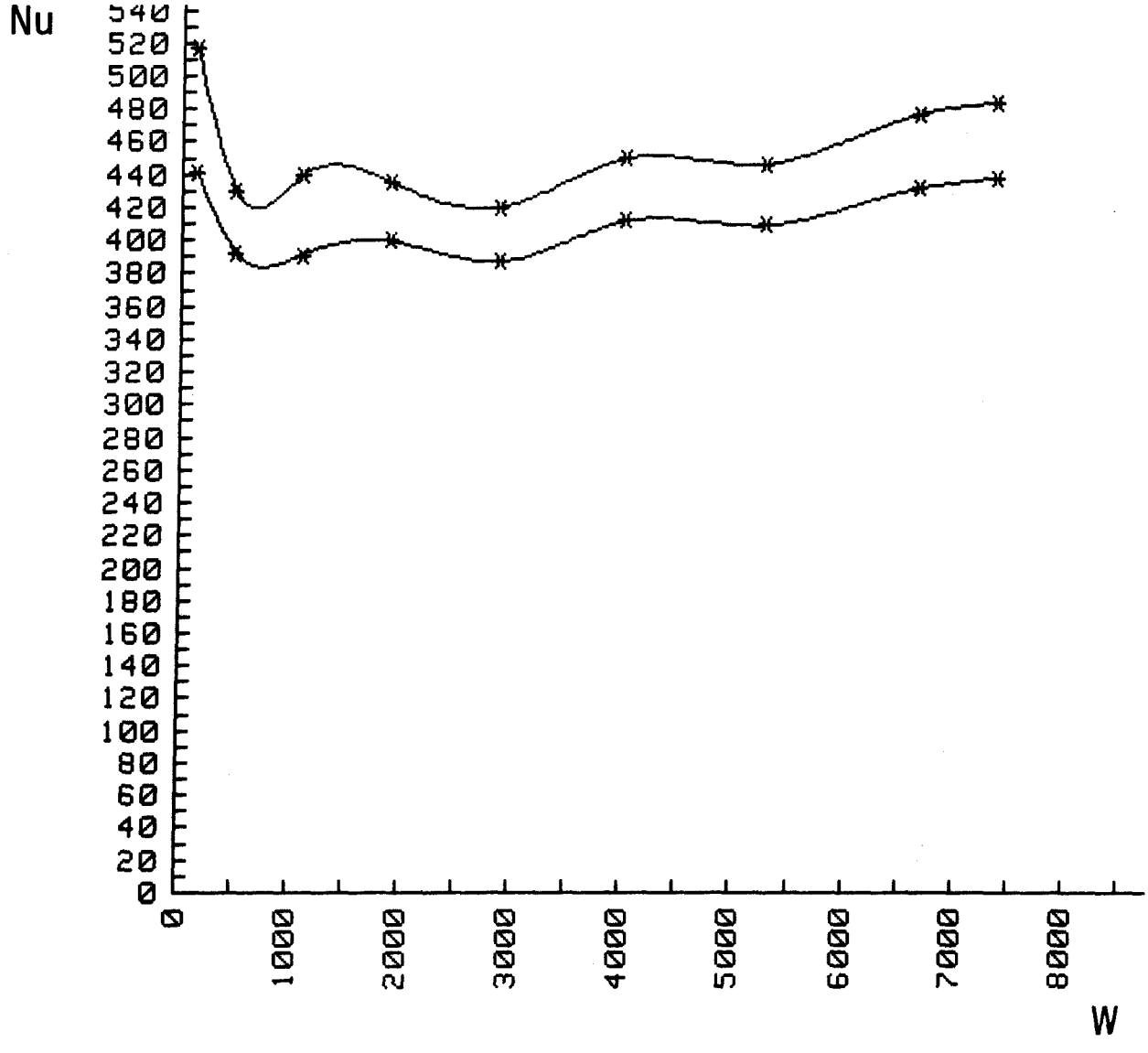

Fig. 23 Behaviour of the Nusselt Number as a function of the heat Production for an average Re=63965 (s=728)

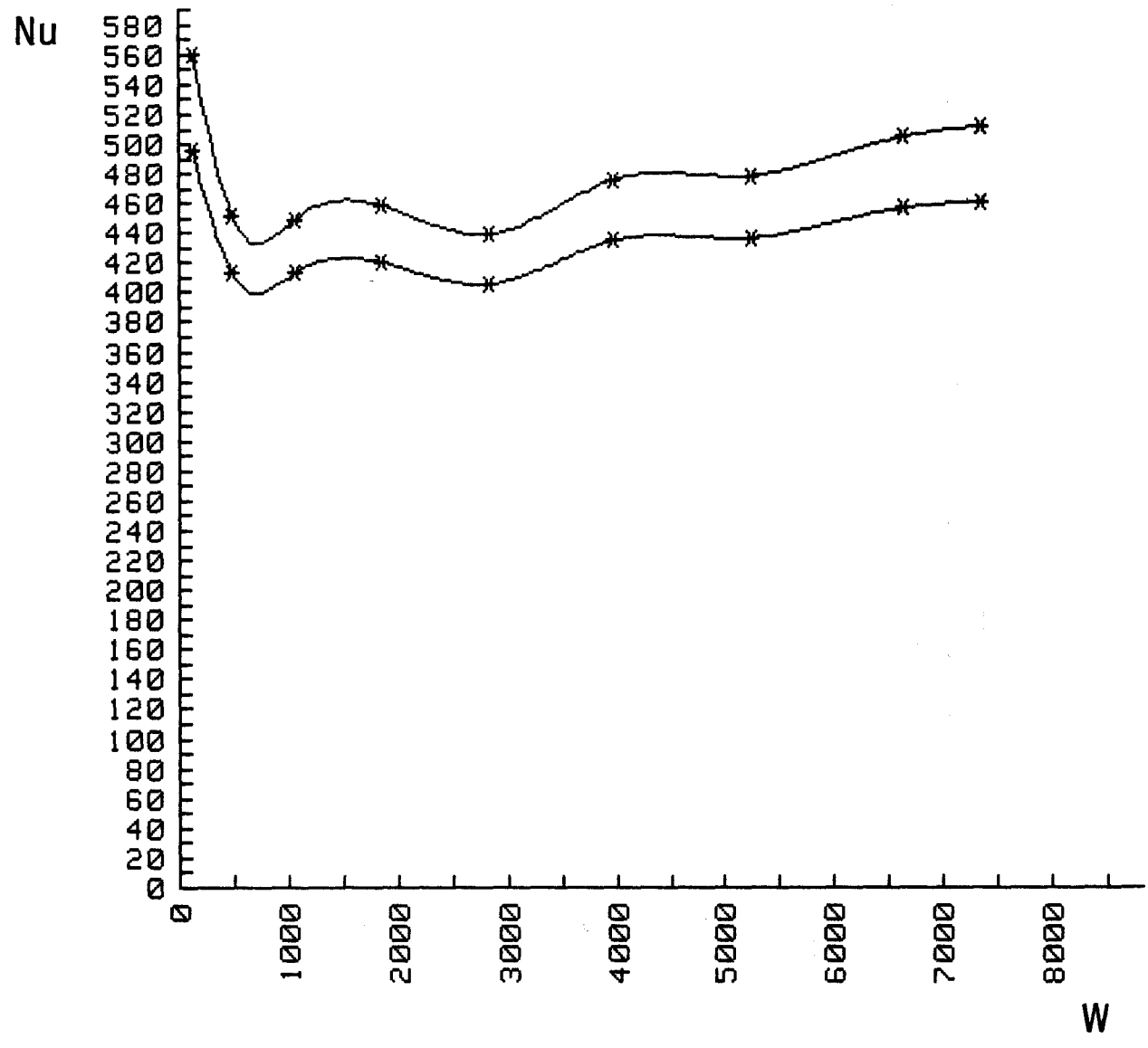

Fig. 24 Behaviour of the Nusselt Number as a function of the heat production for an average Re = 71962 (s = 769).

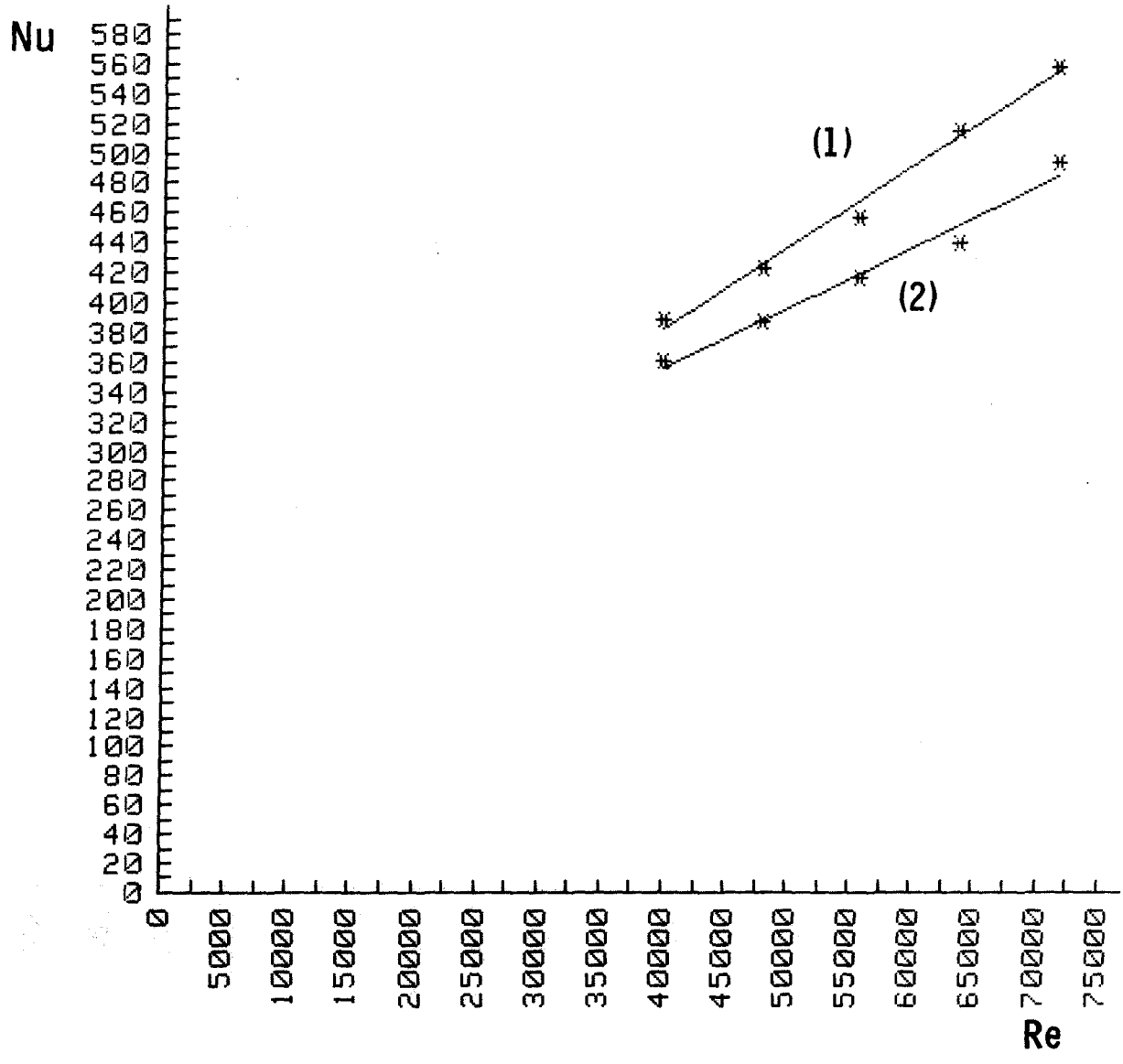

1 - $Nu = 167,8 + 5,43 \cdot 10^{-3} Re$

2 - $Nu = 197,5 + 4,02 \cdot 10^{-3} Re$

Fig. 25 Behaviour of the Nusselt Number as a function of Reynolds for an average W = 121 w.

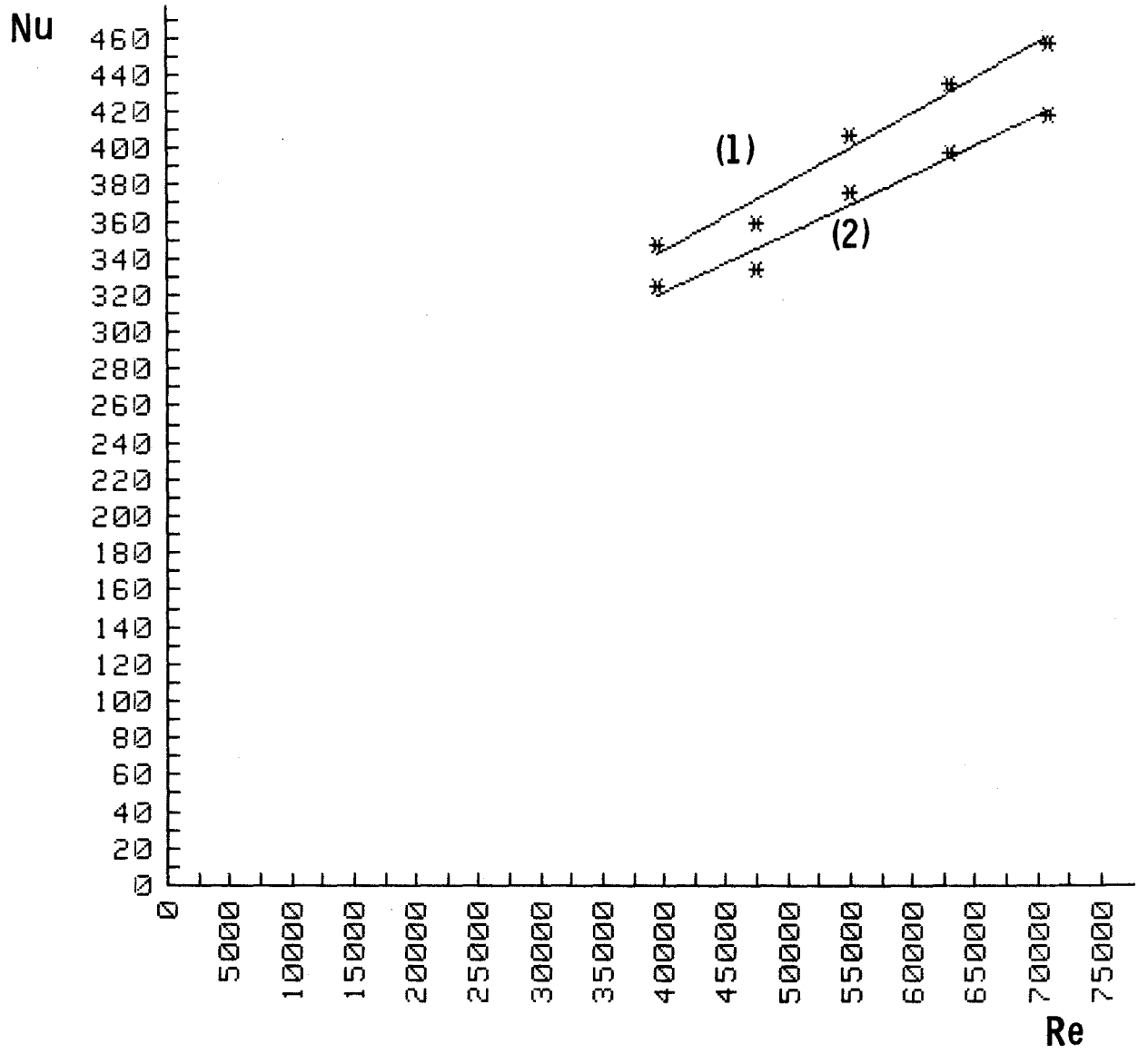

1. $Nu = 195,0 + 3,65 \cdot 10^{-3} Re$
2. $Nu = 196,5 + 3,06 \cdot 10^{-3} Re$

Fig. 26 Behaviour of the Nusselt Number as a function of Reynolds for an average W=483 w.

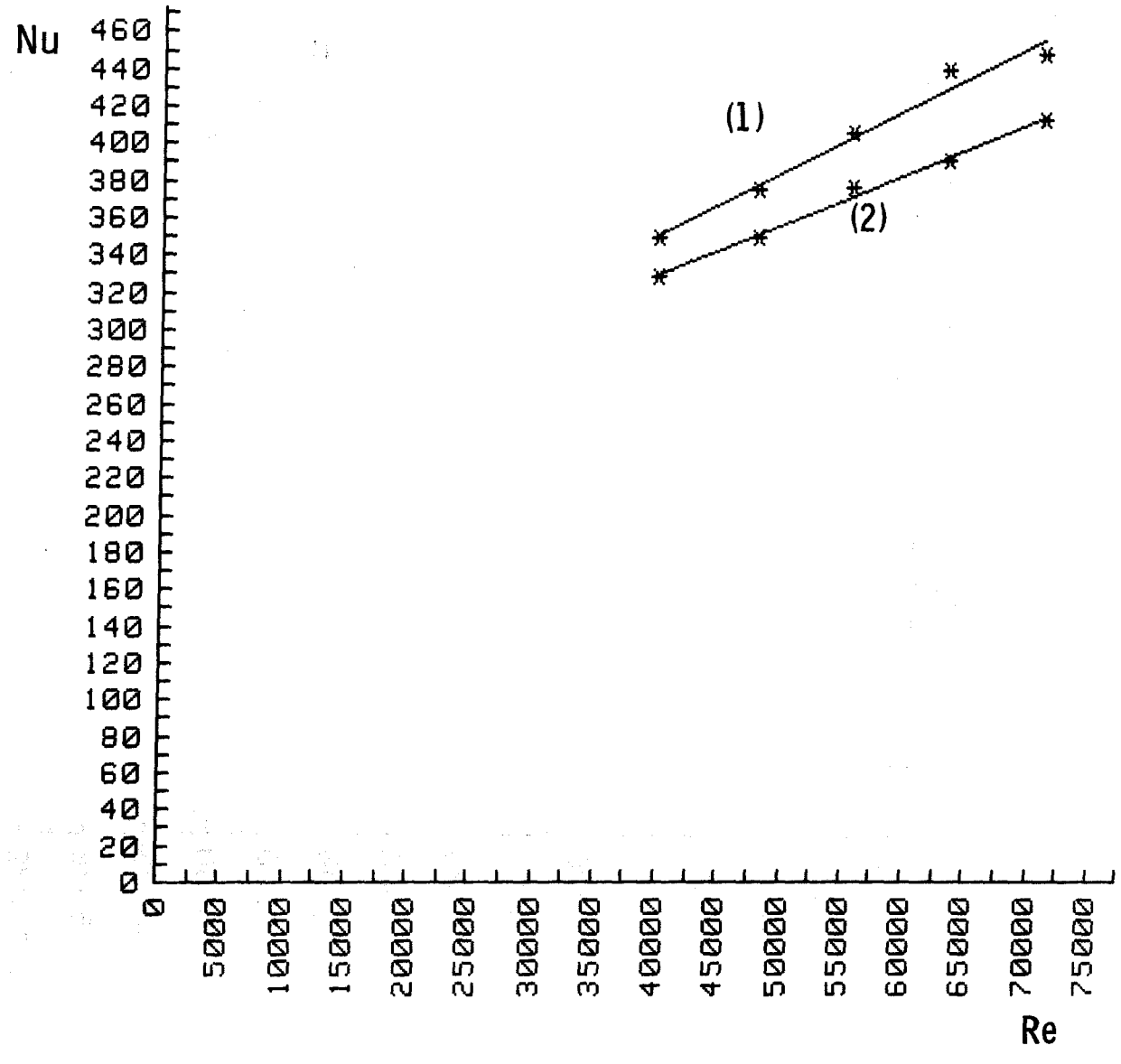

1. $Nu = 217,9 + 3,34 \cdot 10^{-3} Re$
2. $Nu = 222,4 + 2,69 \cdot 10^{-3} Re$

Fig. 27 Behaviour of the Nusselt Number as a function of Reynolds for an average W = 1068 w (s=1,92)

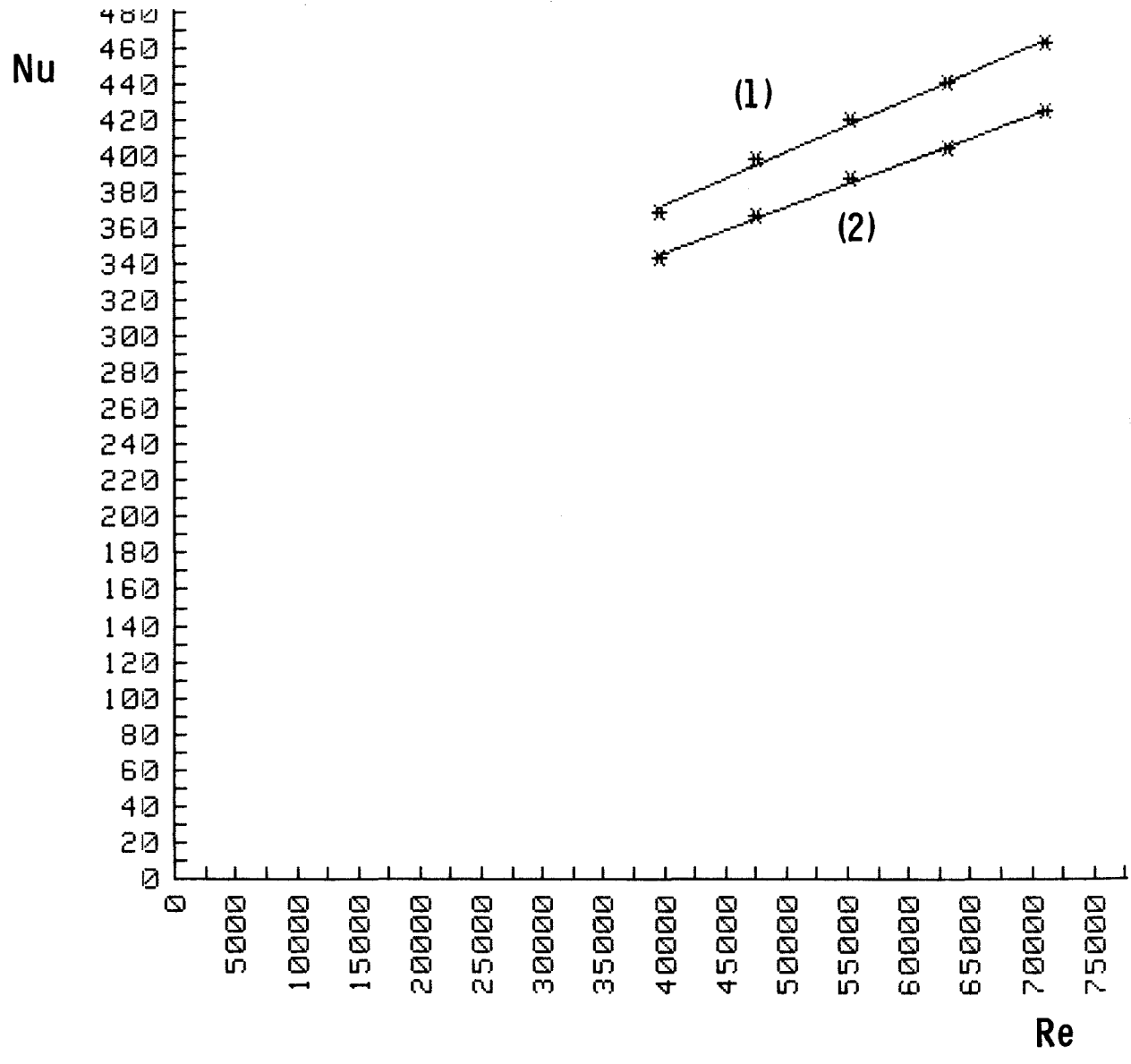

1. $Nu = 255,8 + 2,85 \cdot 10^{-3} Re$
2. $Nu = 245,3 + 2,45 \cdot 10^{-3} Re$

Fig. 28 Behaviour of the Nusselt Number as a function of Reynolds for an average W = 1860 w (s = 4,15).

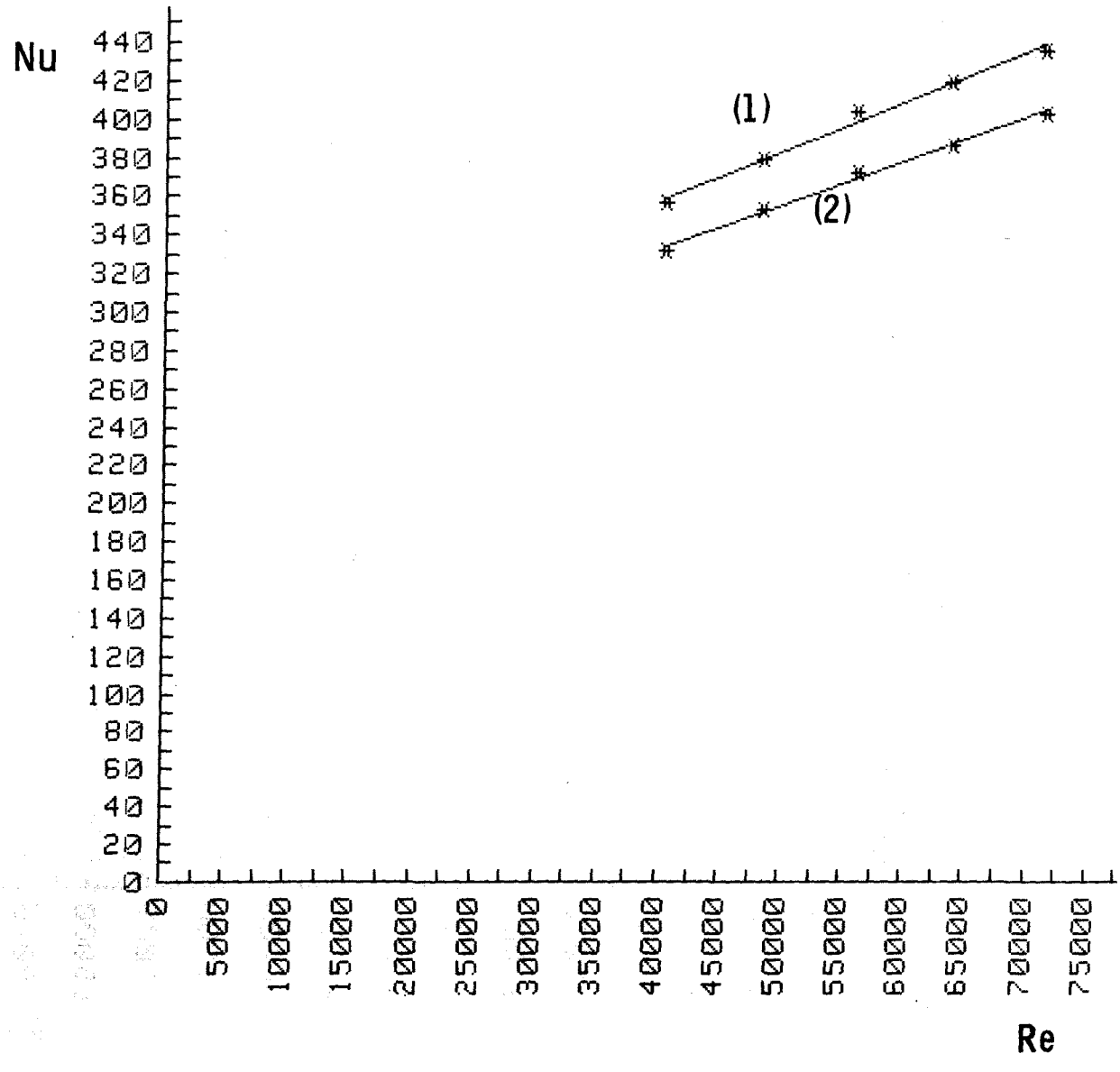

1. $Nu = 256,8 + 2,56 \cdot 10^{-3} Re$
2. $Nu = 244,3 + 2,24 \cdot 10^{-3} Re$

Fig. 29 Behaviour of the Nusselt Number as a function of Reynolds for an average W = 2832 w (9,26)

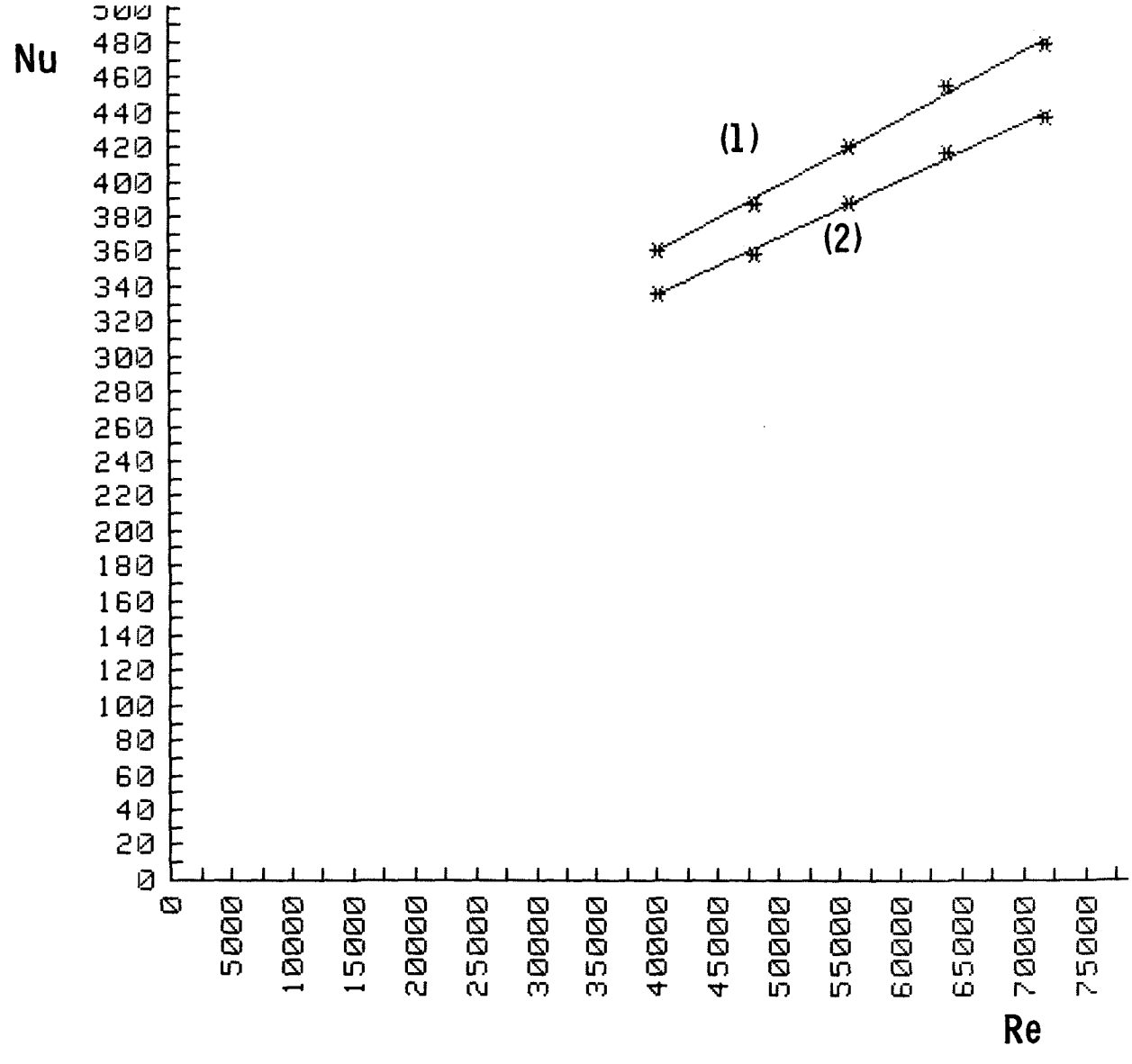

1. $Nu = 207,7 + 3.72 \cdot 10^{-3} Re$
2. $Nu = 204,7 + 3.19 \cdot 10^{-3} Re$

Fig. 30 Behaviour of the Nusselt Number as a function of Reynolds for an average W = 3963 w. (S=22,9)

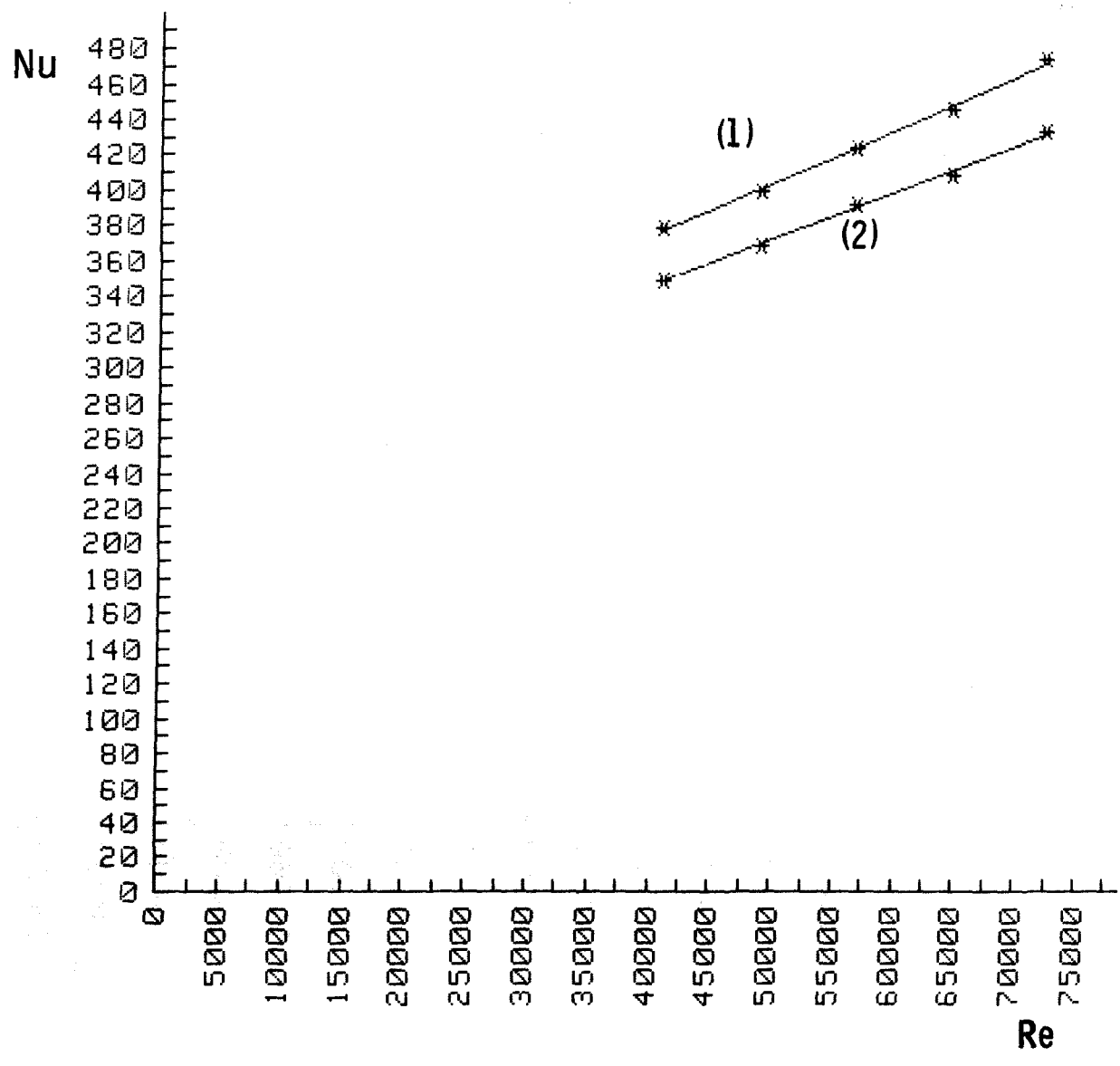

1. $Nu = 255,0 + 3,00 \cdot 10^{-3} Re$
2. $Nu = 242,8 + 2,61 \cdot 10^{-3} Re$

Fig. 31 Behaviour of the Nusselt Number as a function of Reynolds for an average W = 5219 w (s=34,54)

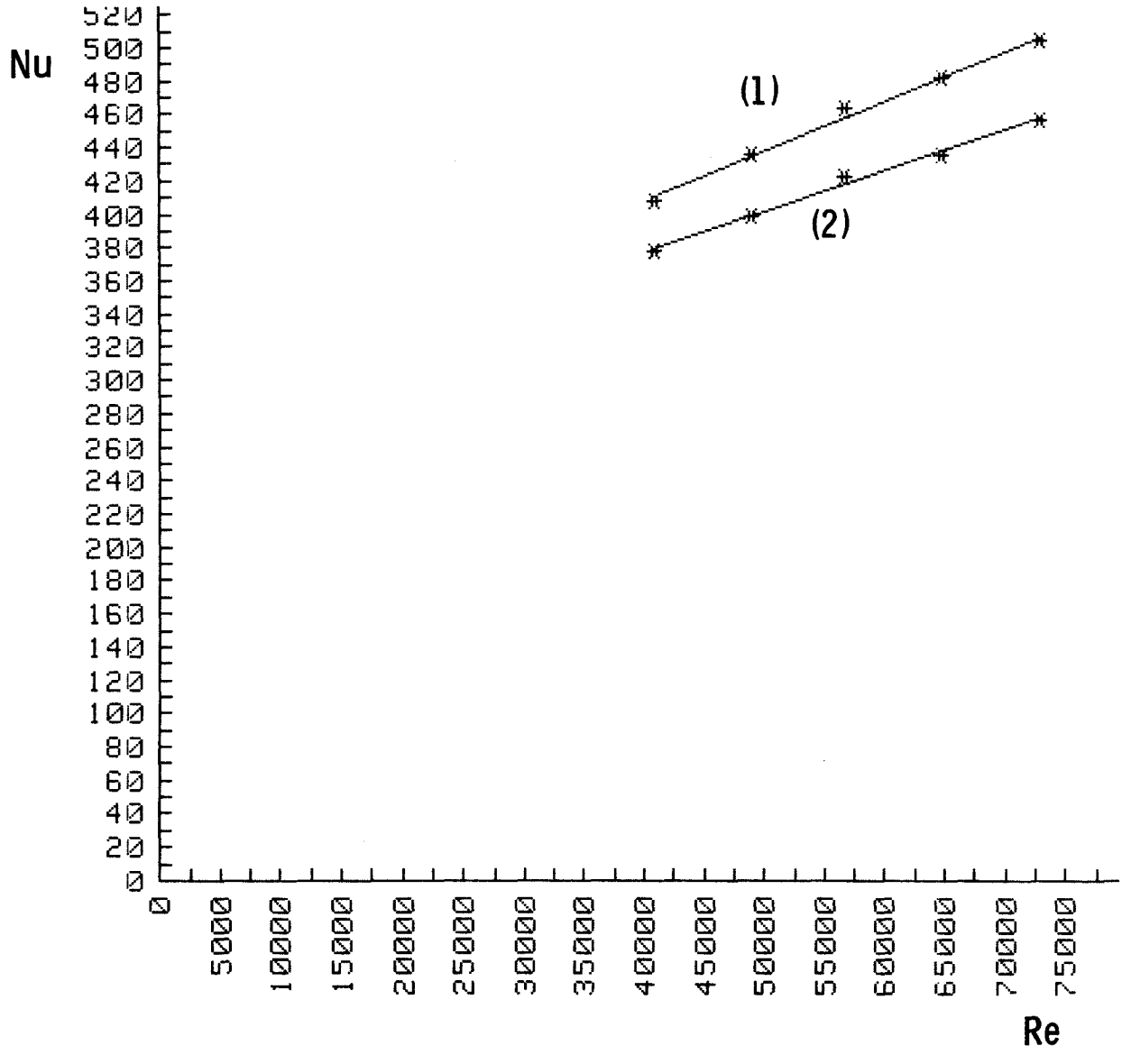

1. $Nu = 291{,}1 + 2{,}89 \cdot 10^{-3} Re$
2. $Nu = 281{,}6 + 2{,}35 \cdot 10^{-3} Re$

Fig. 32 Behaviour of the Nusselt Number as a function of Reynolds for an average W = 6607 N (s = 46,96)

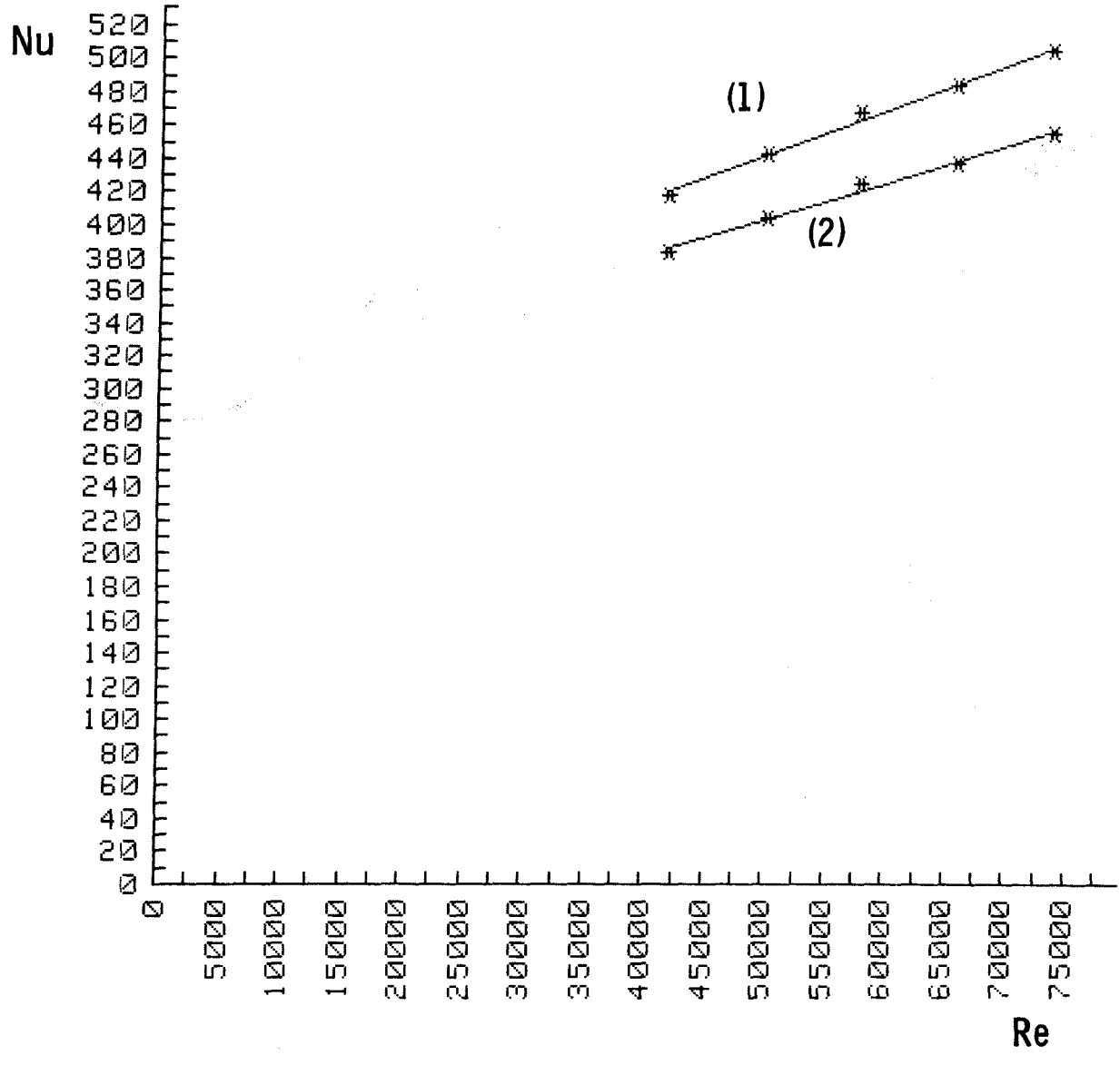

1. $Nu = 309,8 + 2,70 \cdot 10^{-3} Re$
2. $Nu = 296,5 + 2,19 \cdot 10^{-3} Re$

Fig. 33 Behaviour of the Nusselt Number as a function of Reynolds for an average W = 7309 w (s=53,1)

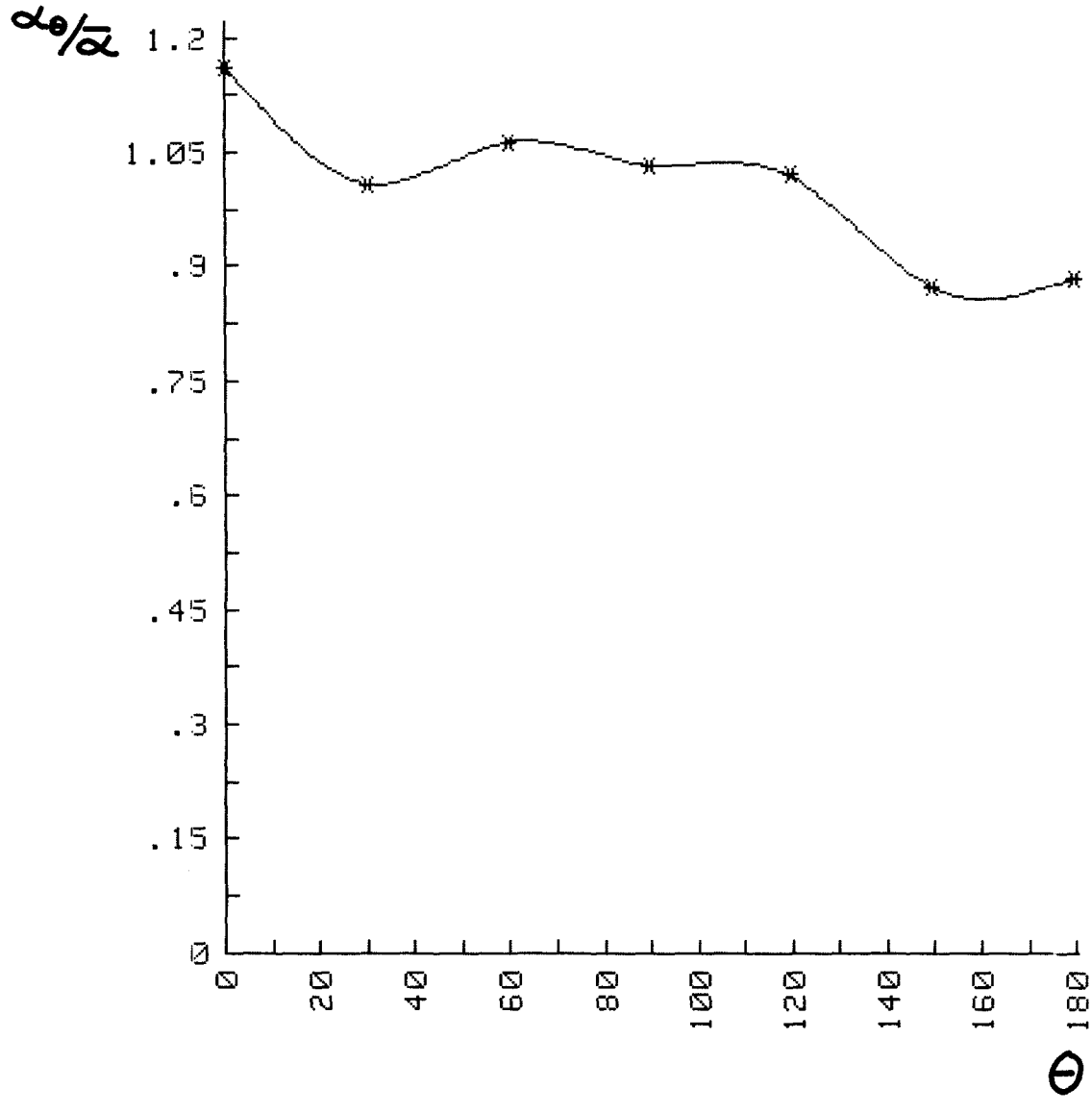

Fig. 34 Local heat transfer coefficient for Re = 41322, W = 7236 w.

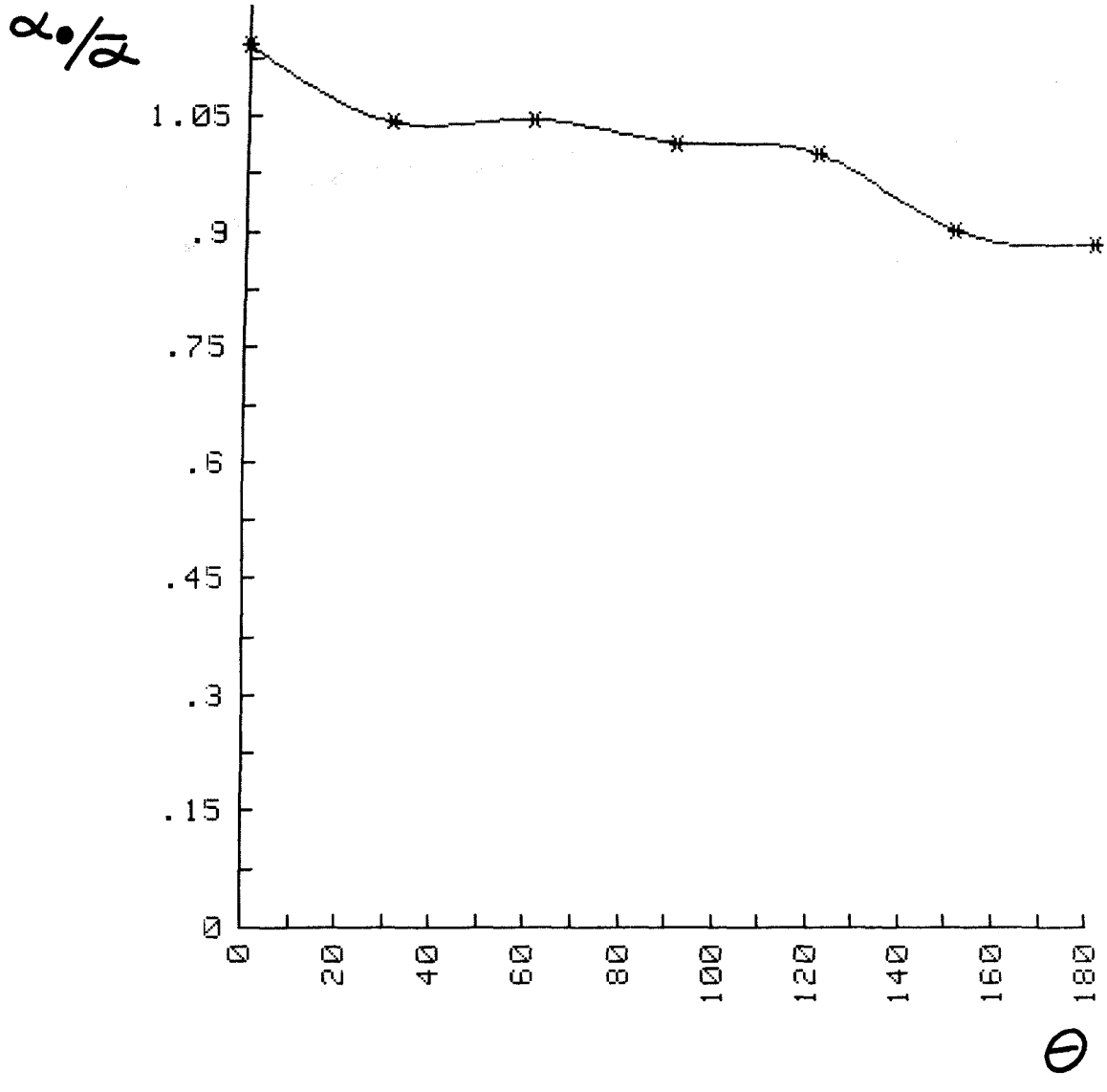

fig. 35 Local heat transfer coefficient for Re = 49360, W = 7280

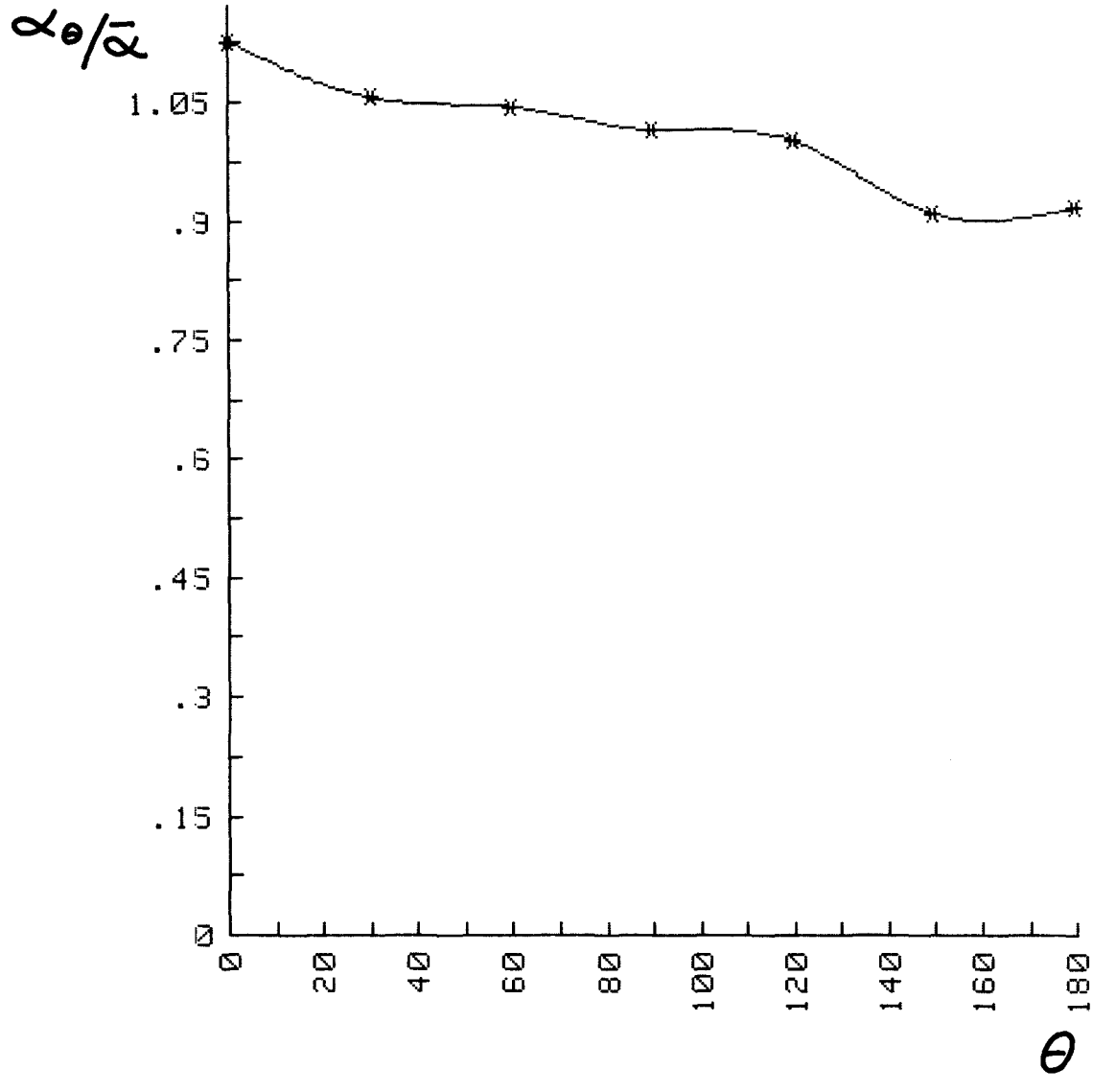

Fig. 36 Local heat transfer coefficient for Re = 57130, W = 7316 w

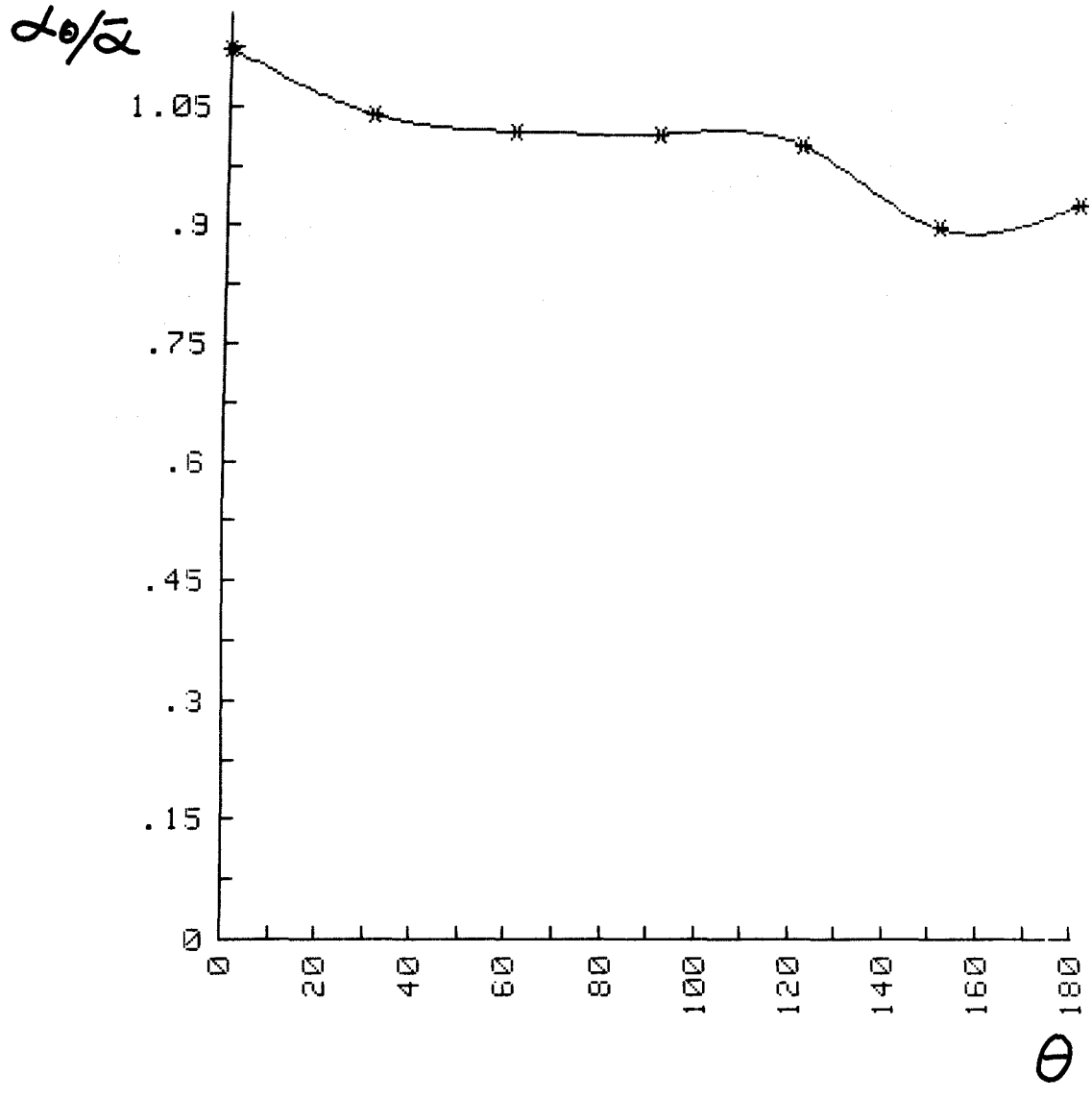

Fig. 37 Local heat transfer coefficient for Re = 65207, W = 7342 w

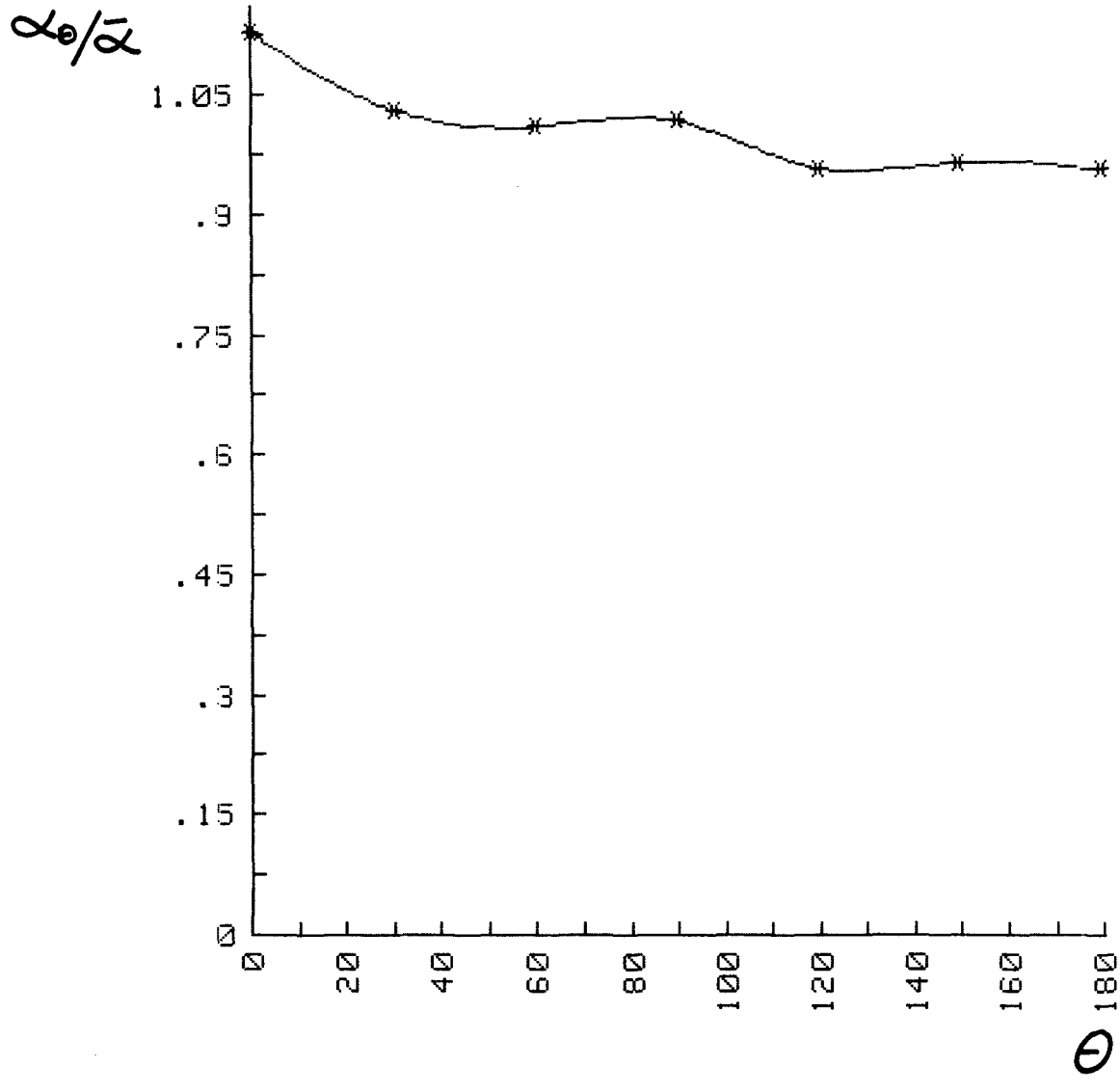

Fig. 38 Local heat transfer coefficient for Re = 73246, W = 7372 w

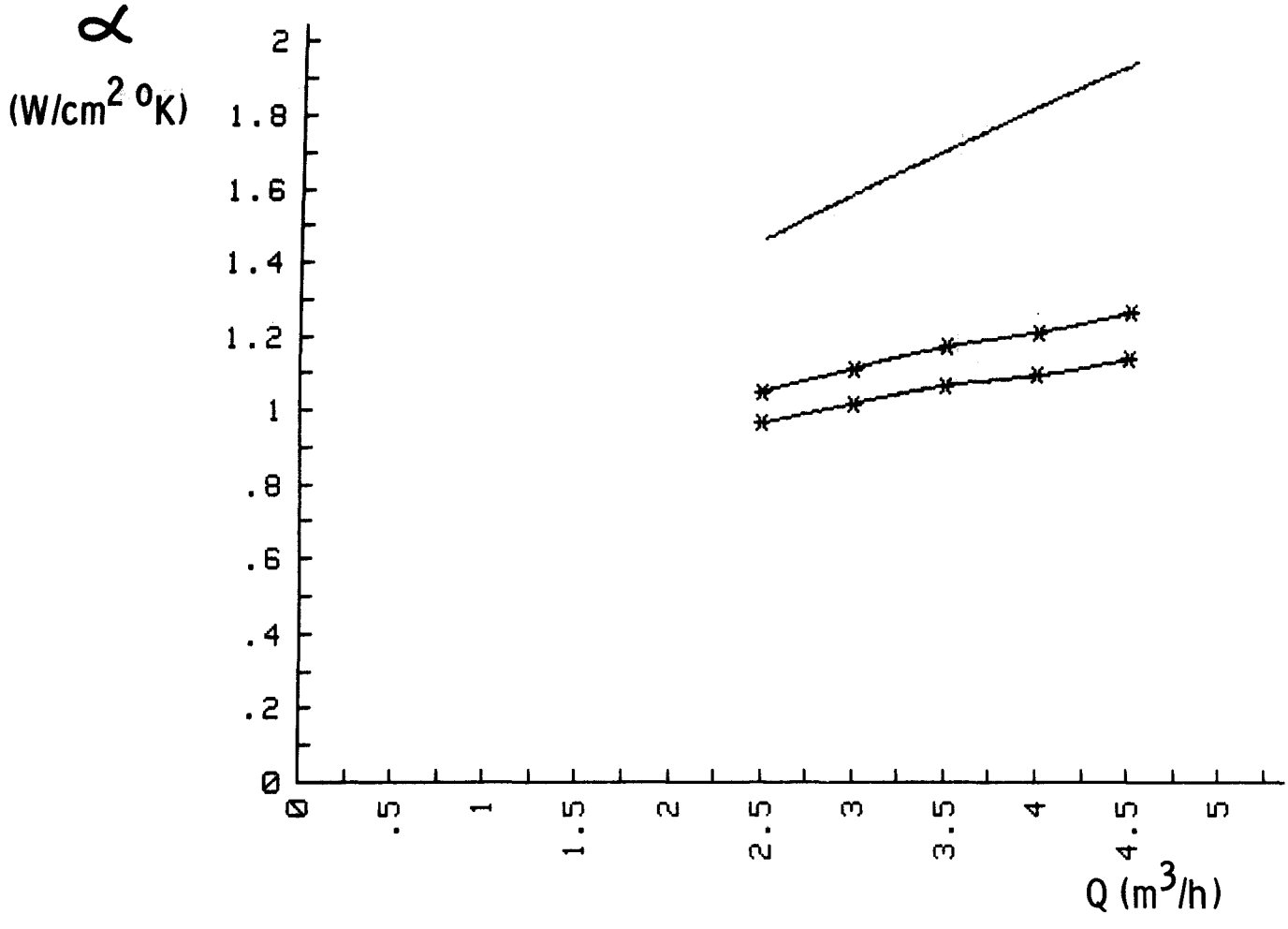

Fig. 39 Comparison of the heat transfer coefficient obtained directly from experiment and calculated with actual datas through Equation (8) (Ref. /7/).

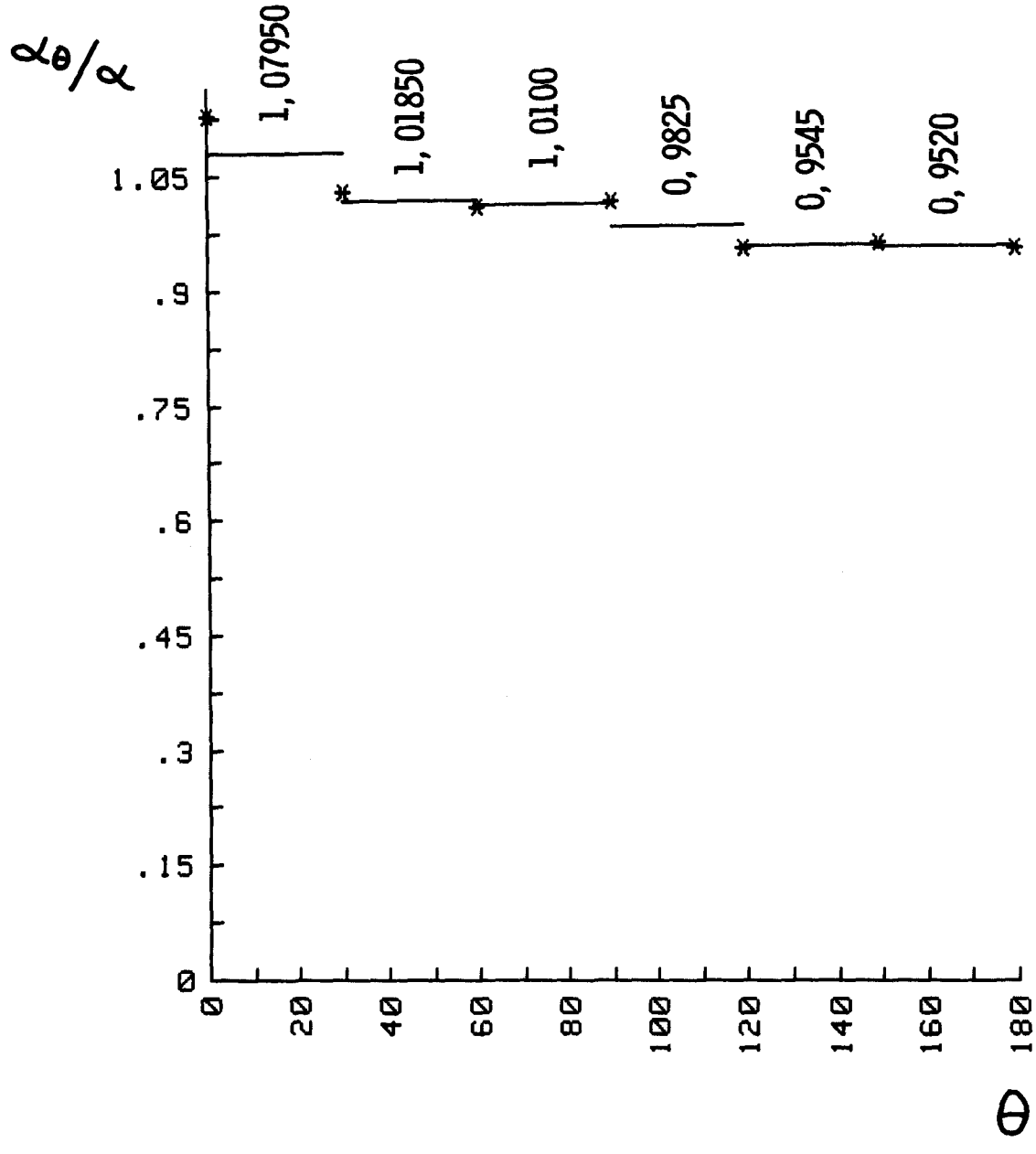

Fig. 40 Stepwise approximation of the local heat transfer coefficient for the program FEMFAM-T. Re = 73246, W = 7372 w.

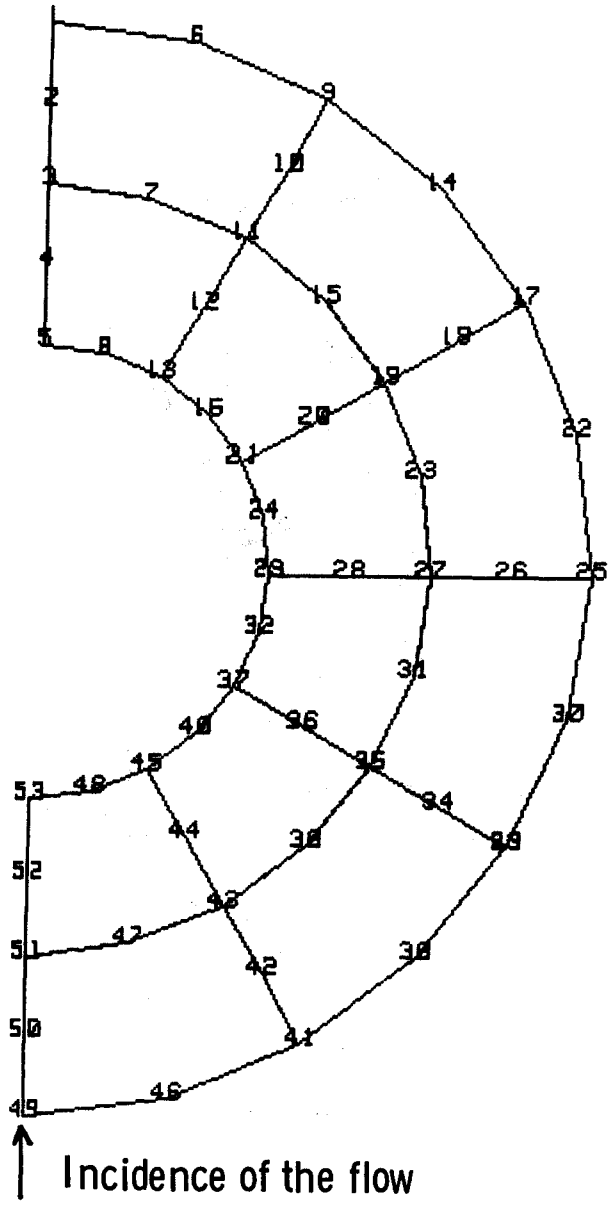

Knotentemperaturen

Knoten	Temperatur				
1	75.92	2	146.47	3	199.71
4	234.06	5	246.69	6	75.93
7	199.70	8	246.63	9	75.82
10	146.32	11	199.52	12	233.78
13	246.40	14	75.49	15	199.13
16	245.98	17	74.71	18	145.28
19	198.57	20	232.88	21	245.53
22	73.73	23	197.83	24	244.94
25	72.79	26	143.58	27	197.01
28	231.56	29	244.27	30	71.89
31	196.37	32	243.62	33	71.48
34	142.23	35	195.71	36	230.19
37	242.93	38	70.88	39	194.96
40	242.22	41	69.45	42	140.48
43	194.19	44	228.89	45	241.73
46	67.84	47	193.56	48	241.34
49	67.86	50	139.27	51	193.18
52	228.24	53	241.19		

Fig. 41 Mesh for the program FEMFAM-T and the list of temperatures in each knot. W = 7372, $\bar{\alpha}$ = 1,272 W/cm^2 k.

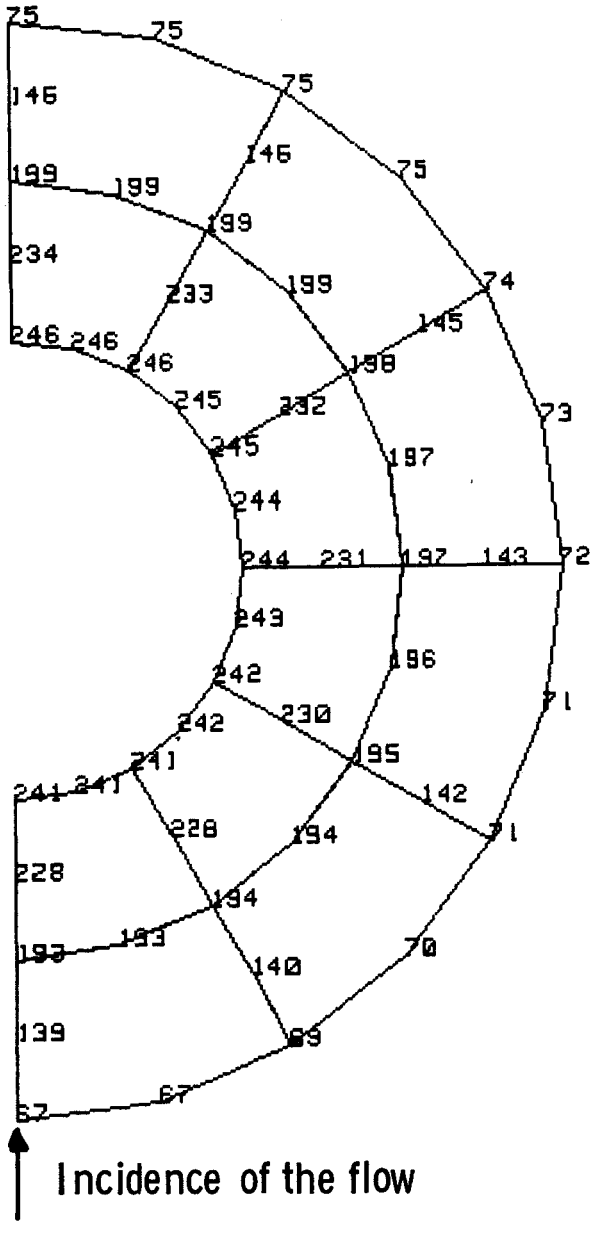

Fig. 42 Representation of the temperatures of the knots on the mesh W = 7372 w, $\bar{\alpha}$ = 1,272 W/cm^{2}k.

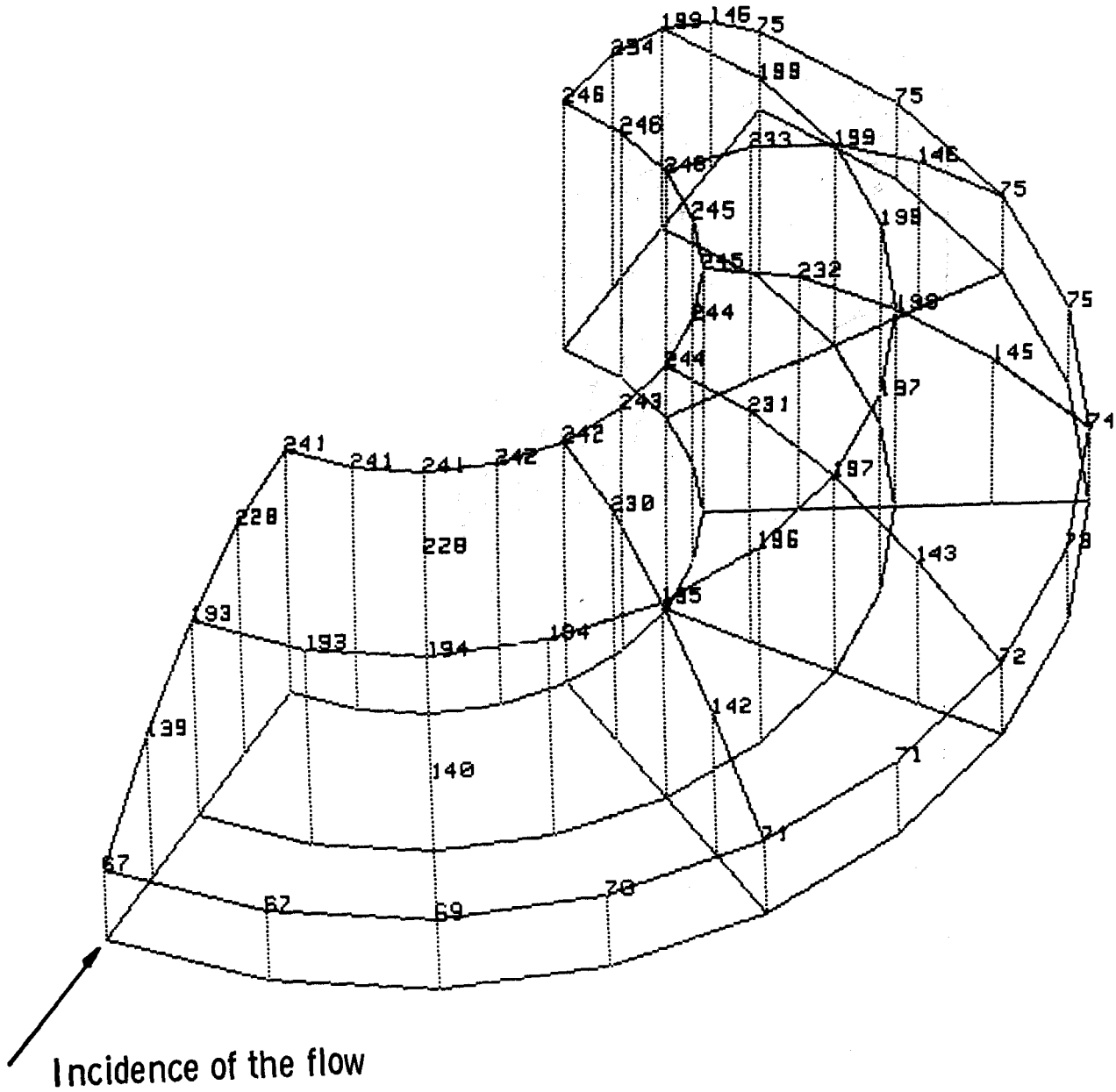

Fig. 43 Relief representation of the temperature vield of the Pin W = 7372 w, $\bar{\alpha}$ = 1,272 W/cm^2 k.

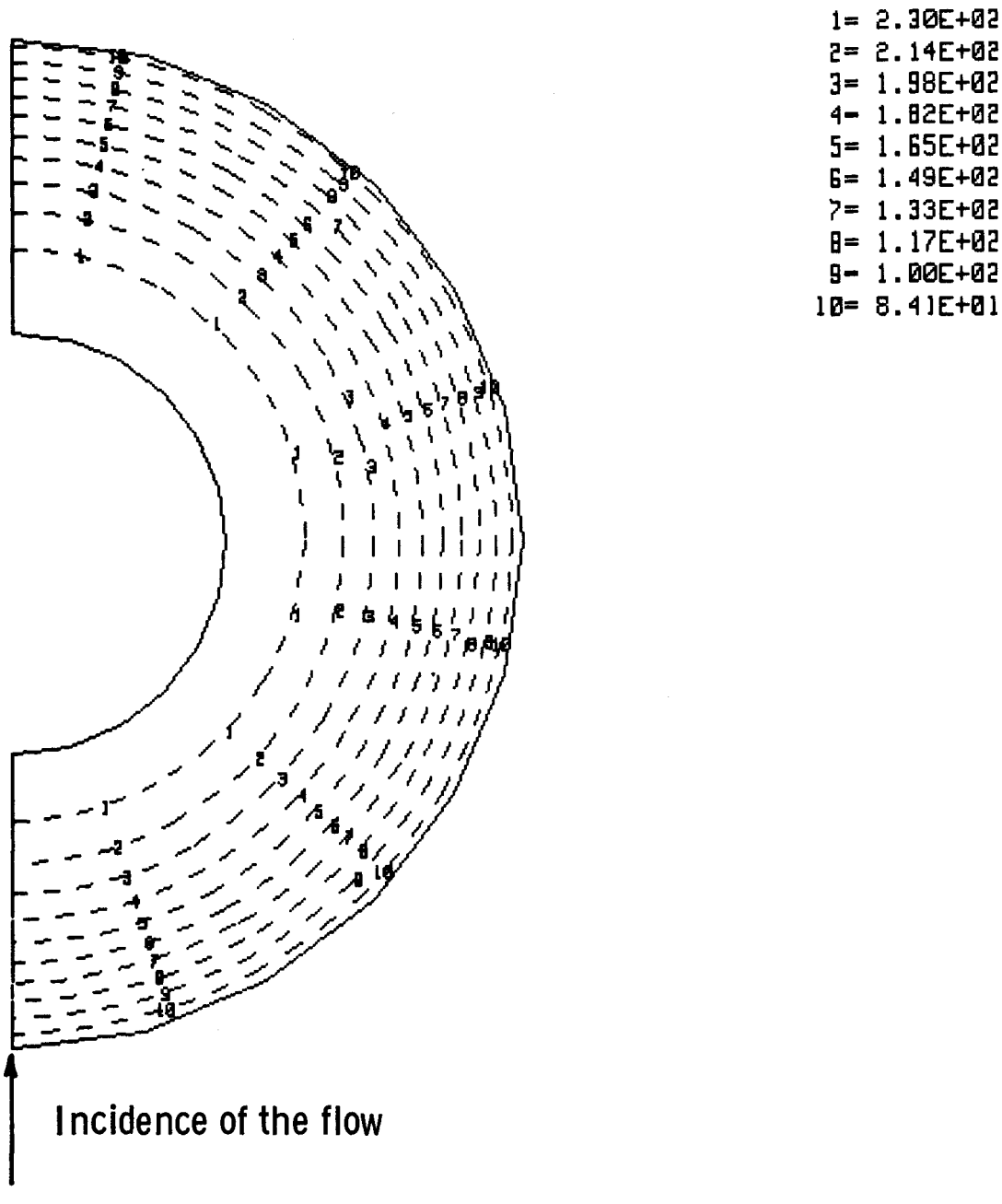

Fig. 44 Isothermic representation of the temperature field of the pin W = 7372 w, $\bar{\alpha}$ = 1,272 W/cm^{2}k.

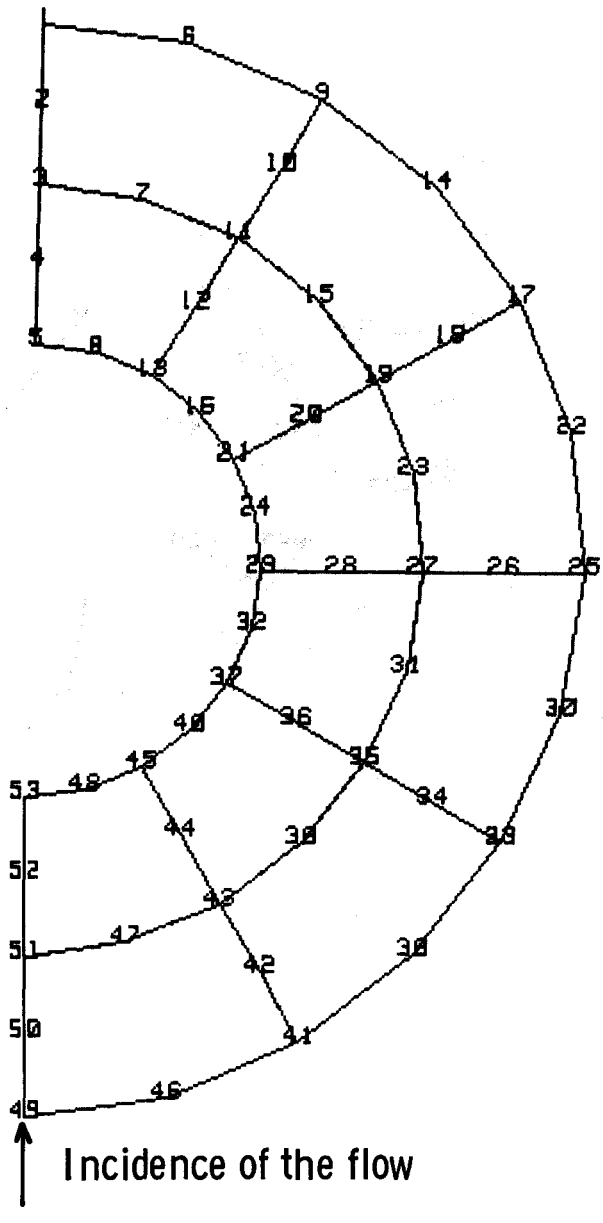

Knotentemperaturen

Knoten	Temperatur				
1	84.32	2	154.85	3	208.06
4	242.39	5	255.01	6	84.33
7	208.04	8	254.94	9	84.19
10	154.66	11	207.84	12	242.08
13	254.69	14	83.81	15	207.41
16	254.23	17	82.97	18	153.53
19	206.79	20	241.10	21	253.74
22	81.91	23	205.99	24	253.09
25	80.89	26	151.68	27	205.10
28	239.65	29	252.36	30	79.92
31	204.39	32	251.64	33	79.44
34	150.19	35	203.67	36	238.15
37	250.89	38	78.76	39	202.84
40	250.11	41	77.19	42	148.25
43	201.98	44	236.71	45	249.56
46	75.44	47	201.30	48	249.13
49	75.44	50	146.93	51	200.89
52	236.00	53	248.97		

Fig. 45 Mesh for the program FEMFAM-T and the list of temperatures in each knot. W = 7372 w, $\bar{\alpha}$ = 1,145 W/cm^2 k.

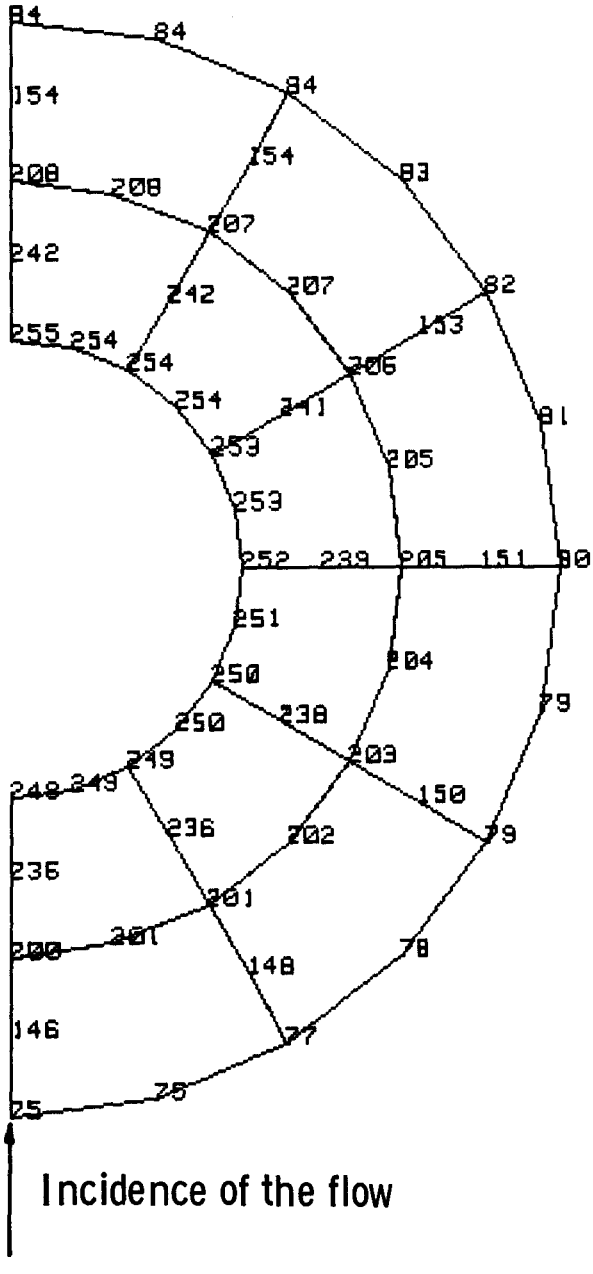

Fig. 46 Representation of the temperatures of the knots on the mesh.
W = 7372 w, $\bar{\alpha}$ = 1,145 W/cm^{2}k.

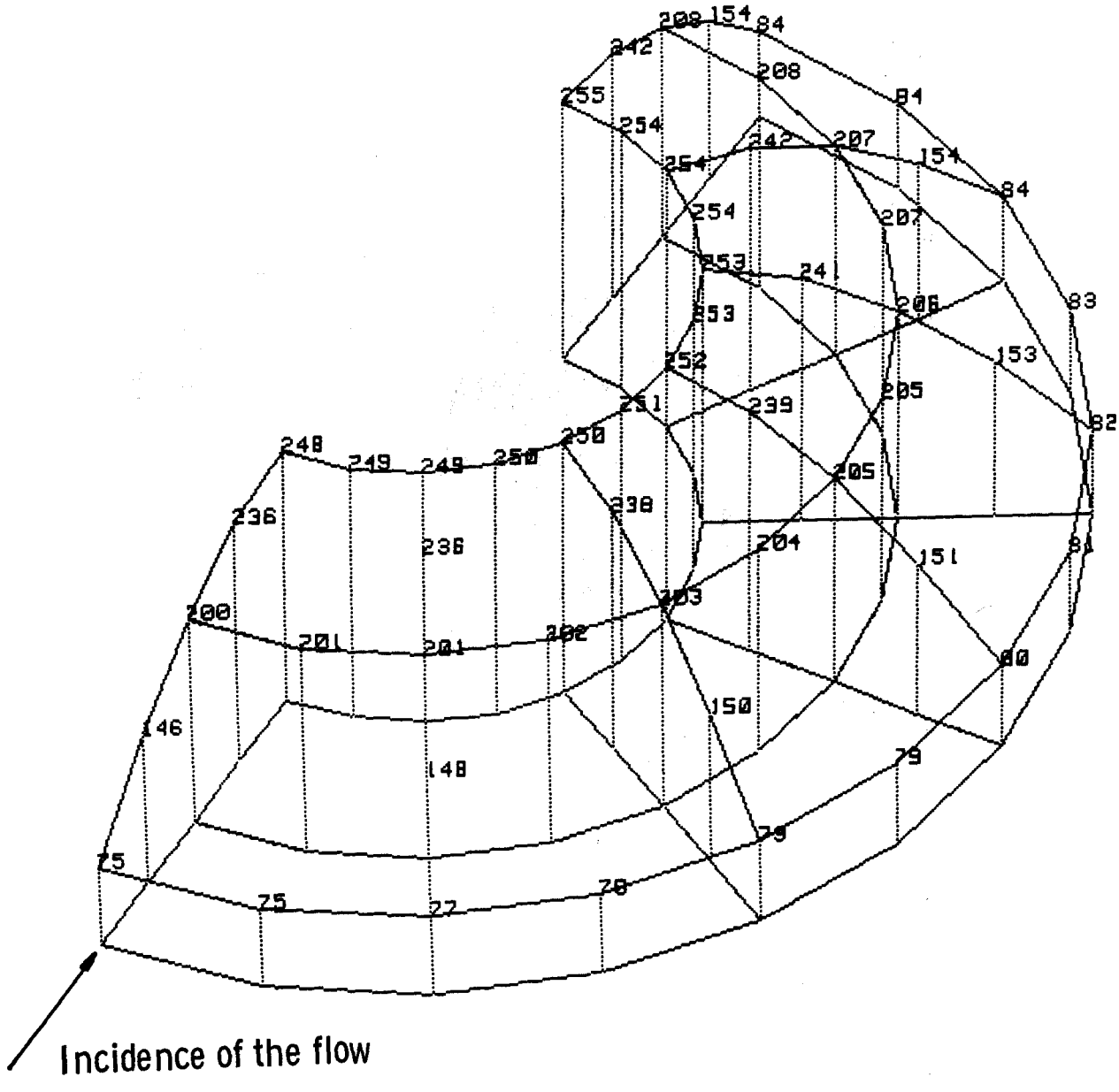

Fig. 47 Reliev representation of the temperature field of the graphit pin - W = 7372 w, $\bar{\alpha}$ = 1,145 W/cm^{2}k.

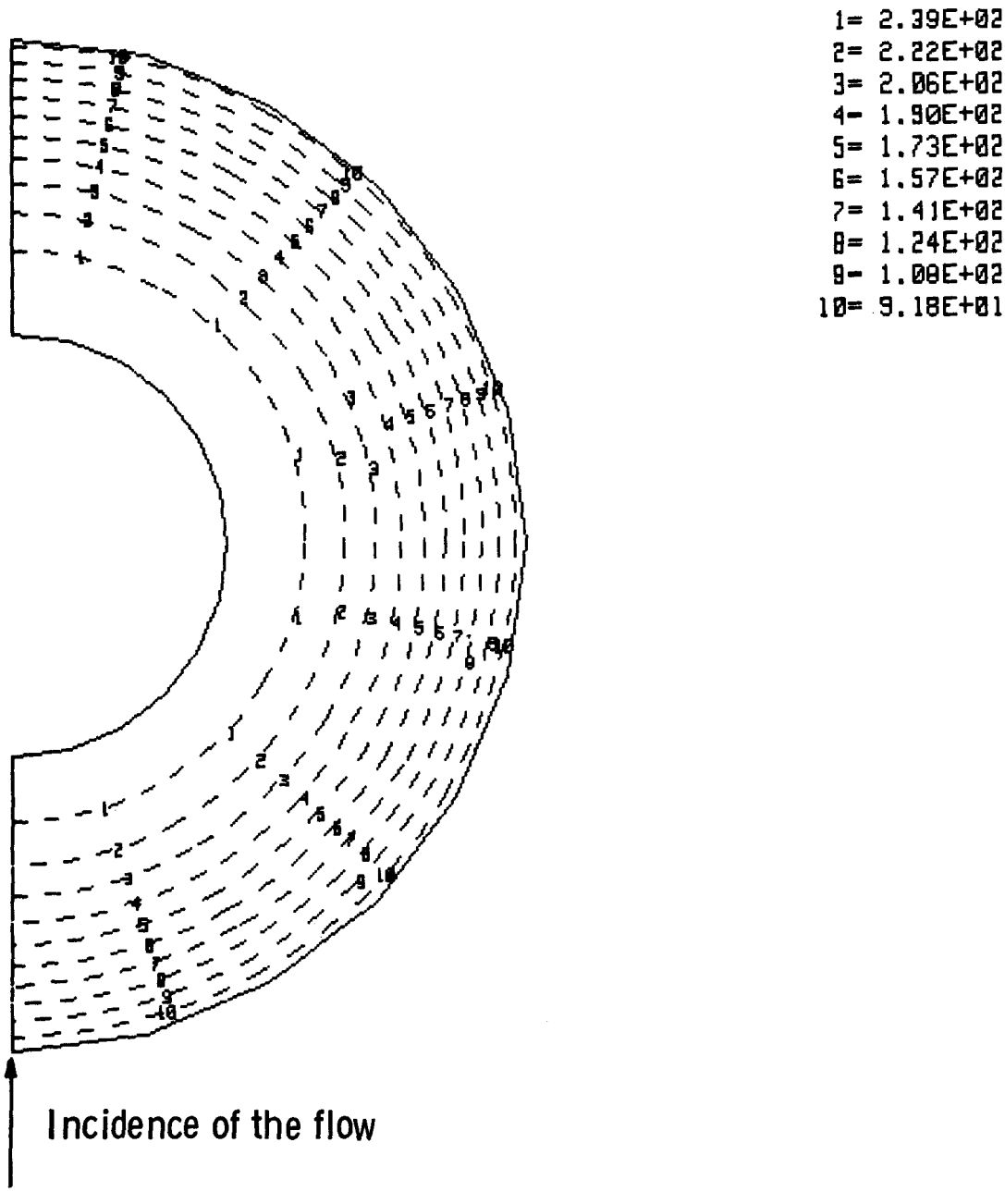

Fig. 48 Isotherm representation of the temperature field of the graphit pin W = 7372 w, $\bar{\alpha}$ = 1,145 W/cm^{2}k.

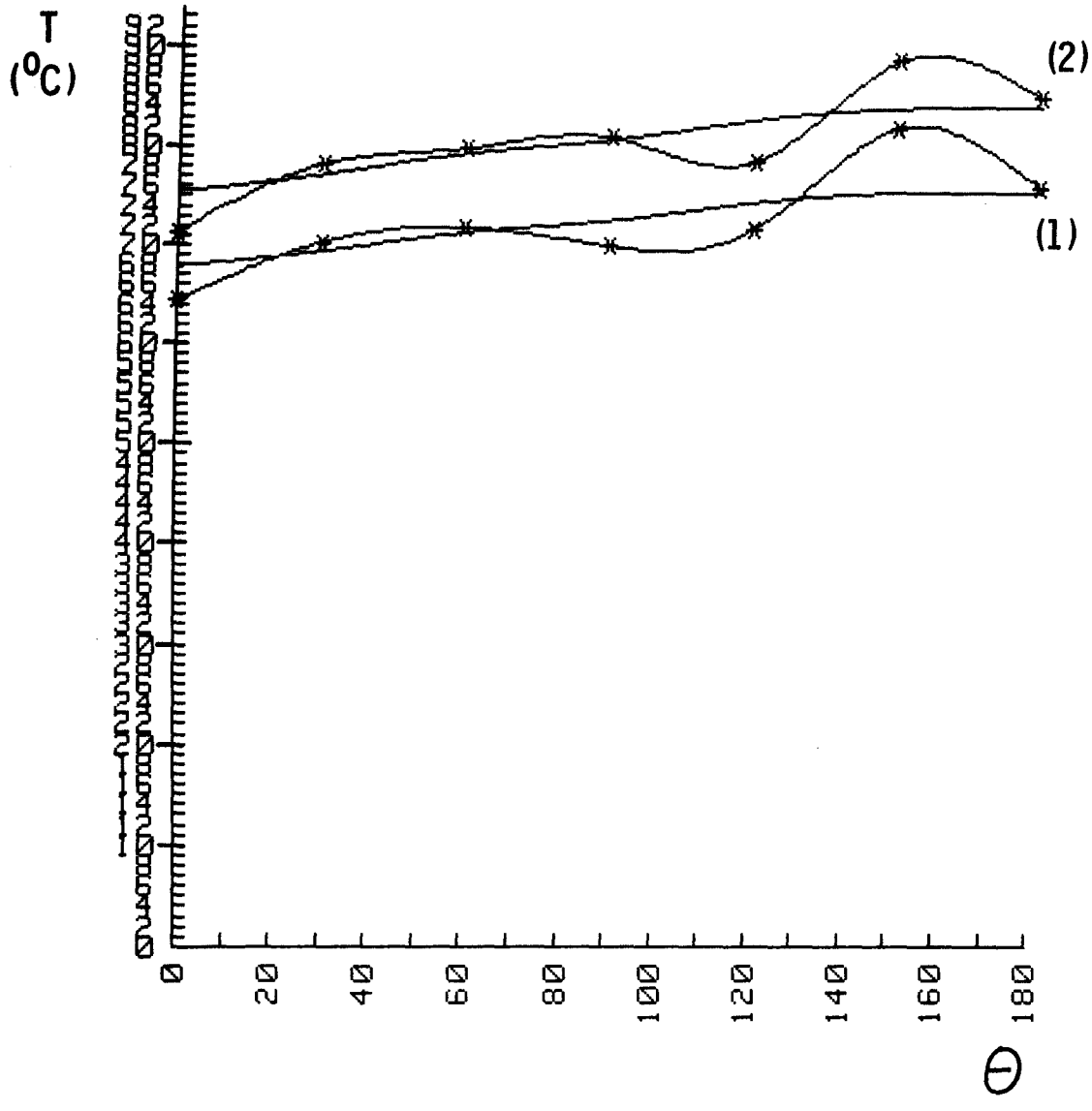

——————— calculated through FEMFAM T

———✱——— measured

Fig. 49 Comparision between the temperature distribution measured and calculated with program FEMFAM-T. W = 7372.
$\bar{\alpha}_1$ = 1,272 W/cm^{2}k, $\bar{\alpha}_2$ = 1,145. W/cm^{2}k.